https://doi.org/10.5194/egusphere-2026-4596
Preprint. Discussion started: 24 August 2026

The Stratified Microbial Carbon Pump: Thermal Stratification Enhances Refractory Dissolved Organic Carbon Production and Stabilizes Carbon in Alkaline Karst Waters through Keystone Microbial Interaction Networks

Yikun Jia[1,2], Junbing Pu[3*], Zaihua Liu[1**], Qiufang He[4], Xinlu Su[3], Tao Zhang[3], Jianhong Li[5], Sibo Zeng[1]

1. State Key Laboratory of Environmental Geochemistry, Institute of Geochemistry, Chinese Academy of Sciences (CAS), Guiyang 550081, China

2. University of Chinese Academy of Sciences, Beijing 100049, China

3. Karst Research Team, Chongqing Key Laboratory of Carbon cycle and Carbon regulation of Mountain Ecosystem, School of Geography and Tourism, Chongqing Normal University, Chongqing, 401331, China

4. Chongqing Key Laboratory of Karst Environment & School of Geographical Sciences, Southwest University, Chongqing 400700, China

5. Key Laboratory of Karst Dynamics, MNR & Guangxi, Institute of Karst Geology, Chinese Academy of Geological Sciences, Guilin, China

** Corresponding author：Junbing Pu*

Address：School of Geography and Tourism, Chongqing Normal University, NO.37, Daxuecheng Central Road, University Town Campus, Shapingba District, Chongqing, 401331, P. R. China

E-mail: junbingpu@163.com

*** Corresponding author Zaihua Liu*

https://doi.org/10.5194/egusphere-2026-4596
Preprint. Discussion started: 24 August 2026

Address: State Key Laboratory of Environmental Geochemistry, Institute of Geochemistry, Chinese Academy of Sciences (CAS), NO.99, West Lincheng Road, Guanshanhu District, Guiyang, 550081, China.

E-mail: liuzaihua@vip.gyig.ac.cn.

Abstract: Recalcitrant dissolved organic carbon (RDOC) represents a persistent fraction of the carbon pool and contributes substantially to regional carbon budgets in terrestrial aquatic ecosystems. Given the substantial carbon sequestration potential of karst waters, elucidating the dynamics and persistence of RDOC is essential for understanding carbon retention in these geologically distinctive environments. Karst reservoirs represent important yet highly complex components of regional carbon cycling. Here, RDOC accumulation and its underlying mechanisms were examined in the Dalongdong (DLD) Reservoir, a dissolved-carbon-rich karst water body, over three contrasting thermal phases: incubating thermal stratification (ITS), obvious thermal stratification (OTS), and mixing (MX). Our results revealed that RDOC dynamics were predominantly regulated by microbial processes rather than benthic carbon inputs. The establishment of thermal stratification generated pronounced physicochemical gradients that facilitated vertical niche partitioning among keystone taxa, thereby regulating DOM bioavailability through taxon-specific metabolic pathways. Bacterial network analysis further indicated that facilitative interactions favored the generation of labile carbon, whereas competitive interactions under environmental stress promoted RDOC accumulation. Notably, the distinctive geochemical conditions of the karst system facilitated Ca–P co-precipitation, resulting in persistent phosphorus

https://doi.org/10.5194/egusphere-2026-4596
Preprint. Discussion started: 24 August 2026

limitation and an elevated C:P ratio in the water column. This nutrient imbalance reduced microbial carbon use efficiency and suppressed extracellular enzyme activities, consequently favoring the conversion of autochthonous labile carbon into more persistent RDOC. Collectively, these findings suggest that the synergistic coupling of the biological carbon pump (BCP) and microbial carbon pump (MCP), reinforced by geochemical phosphorus sequestration, represents an important mechanism underlying long-term carbon retention in alkaline, calcium-rich aquatic systems. Our findings further demonstrate that karst-specific geochemical conditions interact with thermal stratification to regulate microbial processes governing carbon persistence. In particular, MCP efficiency appears to be modulated by carbonate-weathering-derived dissolved inorganic carbon (DIC), providing mechanistic insights into the enhanced carbon sequestration capacity of geologically distinctive inland waters. Protecting these highly efficient carbon-sequestering ecosystems may therefore contribute to atmospheric CO_2 removal and provide an additional pathway for advancing global climate mitigation.

Keywords: Refractory dissolved organic carbon, Thermal stratification, Bacteria interactions, Carbon Sink, Microbial Carbon Pump

1. Introduction

Carbonate rock weathering transfers atmospheric and soil-derived CO_2 into DIC, which is subsequently transported into karst aquatic systems, including rivers, lakes, and reservoirs **(Liu et al., 2011)**. Within karst systems, carbonate dissolution consumes CO_2 from CO_2-rich water while

https://doi.org/10.5194/egusphere-2026-4596
Preprint. Discussion started: 24 August 2026

simultaneously producing mobile DIC according to the reaction $CaCO_3 + CO_2 + H_2O \rightarrow Ca^{2+} + 2HCO_3^-$ **(Liu et al., 2018)**. This CO_2 consumption and subsequent DIC transport constitute the fundamental mechanism underlying the karst carbon sink. In contrast to non-karst landscapes, carbonate weathering provides a distinctive and potentially sustained pathway for the transfer of inorganic carbon through terrestrial aquatic systems. Global carbon budget assessments suggest an unresolved uncertainty of approximately 0.4–1.2 Pg C yr^{-1} in terrestrial carbon sinks, with the karst carbon sink potentially accounting for an important fraction of this so-called "missing carbon sink"**(Harris et al., 2021; Houghton and Nassikas, 2017; Friedlingstein et al., 2021; Friedlingstein et al., 2022; Friedlingstein et al., 2023)**. China contains the largest extent of karst landscapes globally, covering approximately 3.46 million km^2, and these extensive karst regions therefore represent substantial potential for carbon sequestration **(Chen et al., 2023)**.

Carbon sequestration in karst systems is governed not only by DIC formation and transport but also by biological processes. The BCP, a concept originally developed in marine biogeochemical research, describes the biological uptake of inorganic carbon through photosynthesis and its subsequent incorporation into organic carbon **(Volk and Hoffert, 1985)**. In karst aquatic environments, aquatic photosynthesis enables the abundant DIC pool to be incorporated into biologically produced organic carbon **(Liu et al., 2018)**. However, the functioning of the BCP in karst waters may differ fundamentally from that in non-karst aquatic systems, where BCP activity is often constrained by the availability of inorganic carbon. Karst waters are typically characterized by high DIC concentrations, elevated pH, and relatively low concentrations of dissolved CO_2, suggesting that conventional carbon-limitation paradigms may

https://doi.org/10.5194/egusphere-2026-4596
Preprint. Discussion started: 24 August 2026

not adequately explain BCP dynamics in these environments. Under such hydrochemical conditions, the fertilizing effect of aqueous CO_2 may stimulate autotrophic organic carbon (AOC) production, thereby strengthening the potential for carbon sequestration **(Shao et al., 2025; Yang et al., 2016)**.

In contrast to the BCP, the MCP represents a complementary biogeochemical pathway through which carbon is retained in aquatic environments via microbial metabolic processes. Through microbial transformation, labile dissolved organic carbon (LDOC) and semi-labile dissolved organic carbon (SLDOC) can be converted into RDOC, which is considerably more resistant to biological degradation. Owing to its persistence, RDOC may remain in aquatic environments for hundreds to thousands of years, thereby contributing to the formation of long-lived and relatively stable carbon reservoirs **(Jiao et al., 2024)**. The MCP framework provides a mechanistic basis for understanding how microorganisms, including bacteria, archaea, and zooplankton, transform bioavailable dissolved organic carbon into more persistent forms through metabolic activity **(Jiao et al., 2024)**. The resulting RDOC commonly exhibits humic-like fluorescent characteristics and possesses molecular structures that are highly resistant to degradation, facilitating its prolonged retention in aquatic systems and contributing to the establishment of stable carbon pools **(Jiao et al., 2024; Jiao et al., 2010)**. Increasing attention has recently been paid to MCP-mediated carbon transformation in karst aquatic environments, including lakes, rivers, and reservoirs. For example, He et al. reported that microbially derived organic carbon (MDOC) represented the predominant accumulated fraction of RDOC in the Lijiang River, while *Sporichthyaceae* and *Novosphingobium* played important roles in organic carbon formation and stabilization before and after the rainy

https://doi.org/10.5194/egusphere-2026-4596
Preprint. Discussion started: 24 August 2026

season **(He et al., 2022)**. In the Honghua Reservoir, Liuzhou, aerobic anoxygenic phototrophic bacteria (AAPB) were found to enhance the stability of the karst carbon sink by reducing the degradation rate of organic carbon and extending its residence time **(He et al., 2022)**. Shi et al. further suggested that microbial community composition and taxon–taxon relationships play substantial roles in determining RDOC production, while keystone taxa such as *Fluviicola* and *Polynucleobacter* may indirectly contribute to its formation by modulating interactions within the microbial community **(Shi et al., 2025)**. Taken together, available evidence indicates that carbon persistence in karst aquatic environments is closely governed by bacterial community organization and the ecological relationships among taxa. However, the carbon sequestration function of karst waters is highly sensitive to environmental variability. Nutrient inputs can reshape phytoplankton community composition **(Caballero et al., 2025; Bao et al., 2022)** and alter microbial metabolic pathways **(Lozupone and Knight, 2007; Bouvy et al., 1998)**, thereby potentially modifying the efficiencies of both the BCP and MCP. Such environmental sensitivity presents a substantial challenge for effective water-resource management and the maintenance of carbon sequestration functions in karst regions.

Lakes and reservoirs constitute major components of inland aquatic ecosystems and are estimated to account for approximately 38% of carbon emissions from aquatic systems, making them substantial contributors to global carbon fluxes **(Tranvik et al., 2009)**. Among these inland water bodies, karst reservoirs are particularly important because they function as transitional interfaces between groundwater and surface water, where carbon cycling is jointly influenced by the characteristics of karst landscapes and aquatic ecosystems **(Goldscheider et al., 2007)**. Unlike

https://doi.org/10.5194/egusphere-2026-4596
Preprint. Discussion started: 24 August 2026

non-karst lakes and reservoirs, where carbon processing is often strongly influenced by terrestrially derived organic matter transported from surrounding catchments, karst reservoirs are characterized by distinctive carbon storage and greenhouse gas emission patterns associated with substantial endogenous primary production. These unique biogeochemical characteristics may consequently result in carbon cycling dynamics that differ markedly from those of non-karst aquatic systems. Thermal stratification has been observed in some karst reservoirs, generating pronounced vertical gradients in hydrochemical and physical conditions. Such spatial heterogeneity can restructure microbial community composition and functional organization, thereby regulating microbial carbon transformation pathways and ultimately influencing carbon cycling within the reservoir **(Pu et al., 2020; Li et al., 2021; Jia et al., 2024)**.

Despite extensive evidence supporting the MCP as a major pathway for persistent carbon preservation in water bodies, the combined effects of physical stratification and karst-specific geochemical conditions, particularly elevated alkalinity and Ca–P co-precipitation, on carbon retention remain insufficiently resolved. We hypothesized that seasonal thermal stratification in karst reservoirs creates a distinctive physicochemical environment that intensifies phosphorus limitation and alters water-column C:P stoichiometry, thereby driving shifts in microbial metabolism and strengthening the functional coupling between the BCP and MCP. To evaluate this hypothesis, we conducted an integrated investigation focusing on three aspects: (1) the responses of keystone bacterial taxa to stratification-induced hydrochemical gradients; (2) the relationships between microbial co-occurrence network stability and DOM bioavailability; and (3) the regulatory roles of geochemical phosphorus sequestration and nutrient stoichiometry in RDOC accumulation

https://doi.org/10.5194/egusphere-2026-4596
Preprint. Discussion started: 24 August 2026

under the distinctive geochemical conditions of karst reservoirs.

Southwestern China is characterized by an exceptionally dense distribution of karst reservoirs. Among these water bodies, the Dalongdong Reservoir (DLD), situated in Shanglin County of Guangxi Zhuang Autonomous Region, is primarily sustained by groundwater inputs within a karst landscape. Its distinctive hydrological and geochemical features provide a favorable natural setting for elucidating carbon dynamics within karst aquatic environments. In particular, the absence of direct surface-river inflow minimizes external hydrological and biogeochemical inputs, while the reservoir is characterized by high alkalinity and elevated DIC concentrations. These hydrochemical features are widely observed across karst regions and make the DLD Reservoir a valuable natural analogue for exploring inorganic-carbon-mediated processes in inland aquatic ecosystems at broader spatial scales. Strong water–rock interactions, together with the seasonal establishment and subsequent disruption of thermal stratification, create pronounced temporal and vertical variability in the reservoir environment. These coupled geological and physical processes provide an appropriate framework for examining how geological conditions interact with physical forcing to regulate carbon sequestration in stratified inland waters.

Against this background, we focused on the DLD Reservoir and combined high-frequency monitoring of thermal stratification with bacterial community co-occurrence network analysis. Specifically, we sought to determine how thermal stratification, within the context of karst geochemistry, influences RDOC formation through changes in the composition of key bacterial taxa and their ecological interactions. By integrating seasonal physical variability with microbial community organization and carbon transformation, this study seeks to clarify the mechanisms

https://doi.org/10.5194/egusphere-2026-4596
Preprint. Discussion started: 24 August 2026

governing the persistence and long-term retention of carbon within karst aquatic systems. More broadly, our findings may provide new insights into the responses of carbon dynamics to ongoing climatic warming across inland aquatic systems characterized by high alkalinity and carbonate-rich geochemistry.

2. Materials and methods

2.1 Study area

Field investigations focused on the DLD Reservoir (23°30′01″–23°40′08″ N, 108°30′02″–108°36′04″ E), a groundwater-dominated karst water body situated in Shanglin County of Guangxi, southwestern China **(Fig. 1)**. Hydrologically, DLD occupies the headwater section of the Qingshui River within the Hongshui River tributary system. Built in 1958 through impoundment of a natural karst valley, the reservoir encompasses a landscape containing interconnected underground cavities, dolines, and rock fractures. Its principal operational purposes are agricultural irrigation and hydroelectric power production, while the associated drainage basin covers approximately 310 km². The impounded water stretches approximately 13 km, generally spans 500-600 m in width, and broadens to more than 1 km at its widest section, corresponding to a water-surface area of 8.05 km². At the lower end of the valley, a 25-m-high earth-rockfill dam impounds approximately 151 million m³ of water at full storage.

The DLD Reservoir is situated within a humid subtropical monsoon zone characterized by marked intra-annual climatic variability. Meteorological records for the previous five years indicate a mean annual air temperature of 22.51 °C and annual rainfall averaging 1,584 mm. Rainfall is

https://doi.org/10.5194/egusphere-2026-4596
Preprint. Discussion started: 24 August 2026

concentrated primarily between April and September, defining the wetter part of the year, while comparatively drier conditions prevail during the remaining months, extending from October to the following March. Intense rainfall events are particularly common from June to August and are typically characterized by high rainfall intensity over relatively short periods. Hydrological records from the Shanglin County Water Resources Management Bureau indicate that annual precipitation in 2023 was 1,378.5 mm, of which 1,196.1 mm occurred during the wet season, corresponding to approximately 90% of the annual total.

Geomorphologically, the DLD Reservoir is situated within a karst peak-cluster depression characterized by canyon-like terrain that generally descends from northwest to southeast. The reservoir receives groundwater primarily through two subterranean rivers, Xialong and Dalongdong. The surrounding watershed is underlain by dolomite of the Yanguan Formation (C1y), limestone of the Liujiang Formation (D2l), and bedded limestone of the Donggangling Formation (D2d). Extensive karstification has produced a complex landscape consisting of peak clusters, karst valleys, dolines, dry valleys, and interconnected cave systems, resulting in highly fragmented terrain and limited areas of level ground. Structurally, the reservoir is located near the convergence of the Damingshan anticline and Qiaoxian syncline. Its shoreline is consequently steep and irregular, with slopes exceeding 45°, making the reservoir particularly susceptible to hydrological fluctuations and erosion processes.

https://doi.org/10.5194/egusphere-2026-4596
Preprint. Discussion started: 24 August 2026

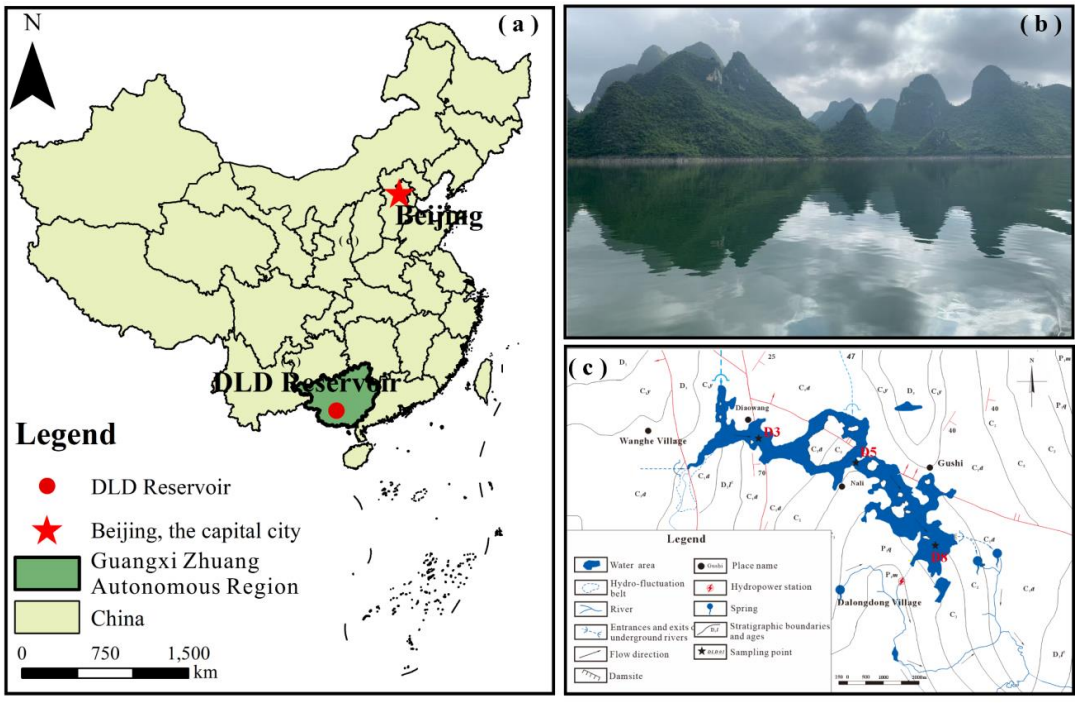

Fig. 1. Overview of the study area and monitoring sites. (a) Location of the DLD Reservoir within China; (b) field photograph of the DLD Reservoir; (c) hydrogeological map of the reservoir area. D3, D5, and D8 denote the monitoring sites positioned in the upper, middle, and lower reaches of the reservoir, respectively.

2.2 Water sample collection and laboratory analysis

2.3.1 Samples collection and pretreatment

Sampling campaigns were carried out during April, August, and November of 2023 across three sections of the DLD Reservoir, with D3, D5, and D8 corresponding to its upper, middle, and lower reaches, respectively **(Fig. 1c)**. These sampling campaigns were scheduled to capture variations associated with reservoir operation and seasonal climatic conditions. At each site, a

https://doi.org/10.5194/egusphere-2026-4596
Preprint. Discussion started: 24 August 2026

peristaltic pump was used to obtain water samples along the vertical water-column profile at intervals of 2.5 m. Fieldwork involved three sequential procedures: water collection, on-site measurements, and subsequent sample preparation. In situ physicochemical parameters were determined using a PONSEL Multy 8320 multiparameter water-quality meter (PONSEL), with measurement precisions of ±0.01 °C for water temperature (WT), ±0.01 units for pH, and ±0.01 mg/L for dissolved oxygen (DO). Chlorophyll-a (Chl-a) concentrations were quantified concurrently with an AP-LITE portable fluorometer manufactured by Aquameter (Aquared, UK); the instrument provides a minimum detection threshold of 0.02 μg/L and a measurement accuracy of ±5%. Before each sampling campaign, all sensors were calibrated following the manufacturer's instructions to ensure measurement quality. Specifically, calibration of the pH electrode employed reference solutions with values of 4.00 and 7.00, while air-saturated water served as the calibration medium for the DO sensor. Three replicate measurements were performed at each sampling point to reduce random measurement error, and their mean was used for subsequent analyses. Additional information on water chemistry and its variation is provided in **Text S1 and Fig. S1**.

Following collection, the dissolved fraction was obtained by filtering each water specimen with a 0.45 μm cellulose acetate filter (Millipore, USA), thereby removing suspended particles. Prior to sample processing, both the filtration unit and filters were conditioned sequentially with 100 mL Milli-Q water (18.2 MΩ·cm), followed by 50 mL of the corresponding filtrate to reduce the risk of contamination. Filtrates were then collected in pre-cleaned high-density polyethylene (HDPE) containers. Preparation of these containers involved immersion in 10% HCl for 24 h, five successive washes with Milli-Q water, and three additional rinses using the corresponding filtered

https://doi.org/10.5194/egusphere-2026-4596
Preprint. Discussion started: 24 August 2026

241 water before sample storage. The prepared filtrates were subsequently analyzed for major metal
242 elements, anions, dissolved organic carbon (DOC), and the stable carbon isotope composition of
243 dissolved inorganic carbon ($\delta^{13}C_{DIC}$).

244 Preservation and storage protocols were tailored to the specific analytical targets. For major
245 cation determination, aliquots were placed in 15 mL HDPE containers pre-cleaned with HNO_3,
246 followed by the addition of 3–5 drops of 7 M high-purity HNO_3 to reduce the pH below 2. For
247 $\delta^{13}C_{DIC}$, 60 mL HDPE containers were filled completely, leaving no headspace, to limit isotopic
248 exchange with atmospheric CO_2. Both DOC and δ^{13}C-DIC aliquots received 1–2 drops of saturated
249 $HgCl_2$ immediately after preparation to inhibit microbial activity. Water intended for chromophoric
250 dissolved organic matter (CDOM) and DOM characterization was stored separately in amber glass
251 containers. Before sampling, these containers underwent three successive washes with potassium
252 dichromate, followed by thorough cleaning with pure water to eliminate residual acid and
253 subsequent air drying. CDOM aliquots were passed through 0.45 μm cellulose acetate filters and
254 subsequently shielded from light to prevent photodegradation. During transportation and storage,
255 all prepared samples were kept refrigerated and protected from light at 4 °C until laboratory
256 measurements were performed.

257

258 **2.3.2 Laboratory analysis and Processing**

259 Cl^-, NO_3^-, and SO_4^{2-} concentrations were determined with a Dionex ICS-900
260 chromatographic system (USA), whereas K^+, Na^+, Ca^{2+}, and Mg^{2+} were quantified on an IRIS
261 Intrepid II XSP spectrometer (Thermo Fisher Scientific, USA) based on inductively coupled

https://doi.org/10.5194/egusphere-2026-4596
Preprint. Discussion started: 24 August 2026

plasma–optical emission spectrometry (ICP-OES). The cation measurements achieved a precision of 0.01 mg/L. Analytical quality was evaluated by examining the balance between the measured anionic and cationic components, with the relative error maintained below 5%.

$\delta^{13}C_{DIC}$ were quantified on a MAT253 mass spectrometric platform equipped with a GasBench continuous-flow interface. Following the phosphoric acid procedure, the obtained isotopic signatures were normalized against the Vienna Pee Dee Belemnite (V-PDB) reference and reported with a measurement uncertainty below 0.15‰. Determination of $\delta^{13}C_{DIC}$ was undertaken by the Institute of Karst Geology, Chinese Academy of Geological Sciences, through its Karst Geological Resources and Environmental Monitoring and Testing Center affiliated with the Ministry of Natural Resources. Laboratory determinations of major anions and cations were completed at the School of Geography Sciences of Southwest University, whereas DOC concentrations were analyzed by the Third Institute of Oceanography under the Ministry of Natural Resources.

TN and TP levels were determined by flow injection analysis with an FIA-6000+ instrument (Jitian Instruments, China). Each determination required a 100 mL aliquot of water without prior filtration, and the analytical procedure achieved a precision of 0.0001 mg/L. These nutrient measurements were undertaken at the School of Geography and Tourism of Chongqing Normal University. For quality assurance, two or three replicates were examined for each specimen; anomalous results were discarded after measurement, and the arithmetic mean of the retained replicates was adopted as the final value for the corresponding parameter.

DOM optical properties were characterized by combining three-dimensional fluorescence and UV–visible absorption measurements at the Chongqing Key Laboratory of Carbon Cycling and

https://doi.org/10.5194/egusphere-2026-4596
Preprint. Discussion started: 24 August 2026

Carbon Regulation in Mountainous Ecosystems affiliated with Chongqing Normal University. A Hitachi F-7000 spectrofluorometer was employed to acquire excitation–emission matrices (EEMs) for CDOM. During spectral acquisition, excitation (Ex) was scanned over 200–500 nm and emission (Em) over 220–600 nm. The respective sampling increments were set at 5 nm and 1 nm, while identical bandwidths of 5 nm were applied to both Ex and Em channels. Spectra were collected at a scanning speed of 2400 nm/min. Instrument performance was checked against ultrapure water before every measurement.

Prior to analysis, all samples were allowed to equilibrate to room temperature and were then placed in a four-window quartz cuvette with a 10 mm optical path length. To minimize cross-contamination, the cuvette was conditioned by rinsing it three times with the corresponding sample before measurement and thoroughly cleaned with ultrapure water three times after each analysis. The acquired EEM spectra were subjected to parallel factor analysis (PARAFAC) using MATLAB 2021 to resolve CDOM fluorescent components and quantify their fluorescence intensities and component loadings. The PARAFAC-derived components were further compared with those available in the OpenFluor database for fluorescence component identification **(Table S1, Fig. S2, and Fig. S3 in Text S2)**. All procedures followed established approaches for CDOM characterization to maintain methodological consistency and facilitate comparison among the resulting data.

UV–visible absorbance measurements were performed on an SP-756P spectrophotometric system, with ultrapure water serving as the reference blank. Before each determination, a two-window quartz cuvette with an optical path length of 10 mm was cleaned by three successive rinses

https://doi.org/10.5194/egusphere-2026-4596
Preprint. Discussion started: 24 August 2026

with ultrapure water. Absorbance was recorded across the 190–800 nm spectral region with a sampling increment of 1 nm.

The absorption coefficient is commonly derived from measured absorbance values to characterize the optical properties of DOM. This conversion is carried out using **Equation (1)**:

$$\alpha\lambda = 2.303\ A\lambda / L \quad \textbf{(1)}$$

$\alpha\lambda$ represents the absorption coefficient at wavelength (λ); L denotes the optical path length of the cuvette (unit: m); $A\lambda$ is the measured absorbance at wavelength λ (dimensionless).

The spectral indicators calculated by the three-dimensional fluorescence spectrometer and the ultraviolet spectrophotometer, along with their temporal and spatial variations, are presented in **Text. S3, Fig. S4 and Fig. S5**.

2.3.3 Bacterial sequencing and analysis

In prokaryotes, the gene coding for 16S rRNA spans approximately 1,500 bp **(Arnemann, 2018)** and contains 10 relatively conserved segments separated by nine highly variable regions designated V1–V9. Sequence heterogeneity within these variable regions provides a molecular basis for distinguishing different microbial taxa. Amplicon-based profiling generally involves recovery of genomic DNA from environmental microbial assemblages, PCR amplification targeting selected variable regions (e.g., V3–V4), and high-throughput determination of the resulting amplicons. The sequence profiles obtained through this procedure allow assessment of taxonomic composition, community-level diversity, and relative representation of bacterial taxa, while also supporting inference of their potential functional characteristics in a given environment.

https://doi.org/10.5194/egusphere-2026-4596
Preprint. Discussion started: 24 August 2026

Accordingly, this molecular strategy can help clarify associations between bacterial assemblages and surrounding environmental conditions or hosts and provide clues regarding their possible ecological functions **(Woo et al., 2008)**.

For bacterial community analysis, amplification targeted the 16S rRNA gene V4 region according to the manufacturer-recommended protocol, employing 515F (5′-GTGYCAGCMGCCGCGGTAA-3′) as the forward primer and 806R (5′-GGACTACHVGGGTWTCTAAT-3′) as the reverse primer. The amplified products were subsequently sequenced for evaluation of bacterial diversity. Initial processing and quality control of the sequence reads were carried out through the QIIME2 bioinformatic workflow, followed by alignment and comparison of the retained feature sequences. Reads occurring fewer than 20 times across the complete dataset were first excluded, after which operational taxonomic units (OTUs) were delineated from the retained sequences using a sequence identity threshold of 97%. The resulting OTU dataset was subsequently analyzed in RStudio (version 4.4.2) to characterize community composition.

2.3.4 Data analysis

Microbial association networks were established from pairwise Spearman correlation coefficients calculated across bacterial OTUs. Before network generation, taxa whose average relative abundance did not reach 0.01% were excluded, and the remaining taxa were subsequently identified manually. Network topology was characterized with the “ggClusterNet” package by calculating the total numbers of nodes and edges, average degree, characteristic path length,

https://doi.org/10.5194/egusphere-2026-4596
Preprint. Discussion started: 24 August 2026

maximum network span (diameter), relative modularity, and the average coefficient of clustering. Graphical representations of these associations were produced in Gephi (version 0.10.1). Potential keystone taxa were identified through their positions within the modular network using "ggClusterNet", based on two node-level parameters: connectivity within a given module (Zi) and connectivity across different modules (Pi). Beyond these structural descriptors, cohesion metrics were calculated to quantify connectivity at the whole-community level. Positive Cohesion reflected the strength of cooperative associations among community members, whereas Negative Cohesion represented competitive or inhibitory relationships.

Associations among DOM components, environmental variables, spectral indices, and bacterial cohesion metrics were evaluated through Spearman correlation analysis and displayed in a correlation heatmap. Mantel tests were additionally applied to examine relationships among the corresponding groups of variables. All correlation analyses were implemented within the R 4.4.3 environment, with "corrplot" (version 0.95) employed for graphical presentation. The magnitude and direction of individual correlations were represented by numerical coefficients and color gradients. Significance levels were marked with one, two, or three asterisks, indicating probability thresholds of $p < 0.05$, $p < 0.01$, and $p < 0.001$, respectively.

Bayesian linear regression models were further developed to assess how environmental conditions, bacterial cohesion, and DOM spectral properties were related to LDOC and RDOC concentrations. The predictor set comprised environmental parameters, Positive and Negative Cohesion metrics, and spectral indicators associated with autochthonous/allochthonous sources and bacterial activity. Model estimation was performed with "rstanarm", whereas "bayesplot" was

https://doi.org/10.5194/egusphere-2026-4596
Preprint. Discussion started: 24 August 2026

employed to visualize the resulting model outputs. An R^2 prior centered at 0.5 was specified, reflecting an initial assumption that the predictors collectively accounted for roughly half of the observed variability. Posterior regression coefficients were then graphically summarized to compare the direction and magnitude of the associations between individual predictors and LDOC or RDOC concentrations.

3. Results

3.1 Thermal stratification of the DLD Reservoir

Research data indicate that the DLD Reservoir is a warm monomictic reservoir **(Hasan et al., 2013)**, exhibiting distinct seasonal variations in its thermal structure **(Jia et al., 2024; Li et al., 2021)**. Based on water temperature profiles and stratification indices (Schmidt Stability Index (SSI) and RWCS/H **(Fig. 2a and b, Text S4**), the DLD Reservoirwas divided into three periods: the incubating thermal stratification (ITS) period in April, with mild stratification; and the obvious thermal stratification (OTS) period in August, featuring stable layering; and the mixing (MX) period in November **(Zhang et al., 2023; Liu et al., 2020)**. The thermocline was absent in November, while it spanned 1.58–6.02 m in April and 1.53-10 m in August **(Fig. 2c)**. Based on these boundaries and sampling at 2.5 m intervals**(Li et al., 2021; Jia et al., 2024)**, the water column was categorized as: epilimnion/surface (0-2.5 m), thermocline/middle (2.5-7.5 m), and hypolimnion/bottom (≥ 7.5 m).

https://doi.org/10.5194/egusphere-2026-4596
Preprint. Discussion started: 24 August 2026

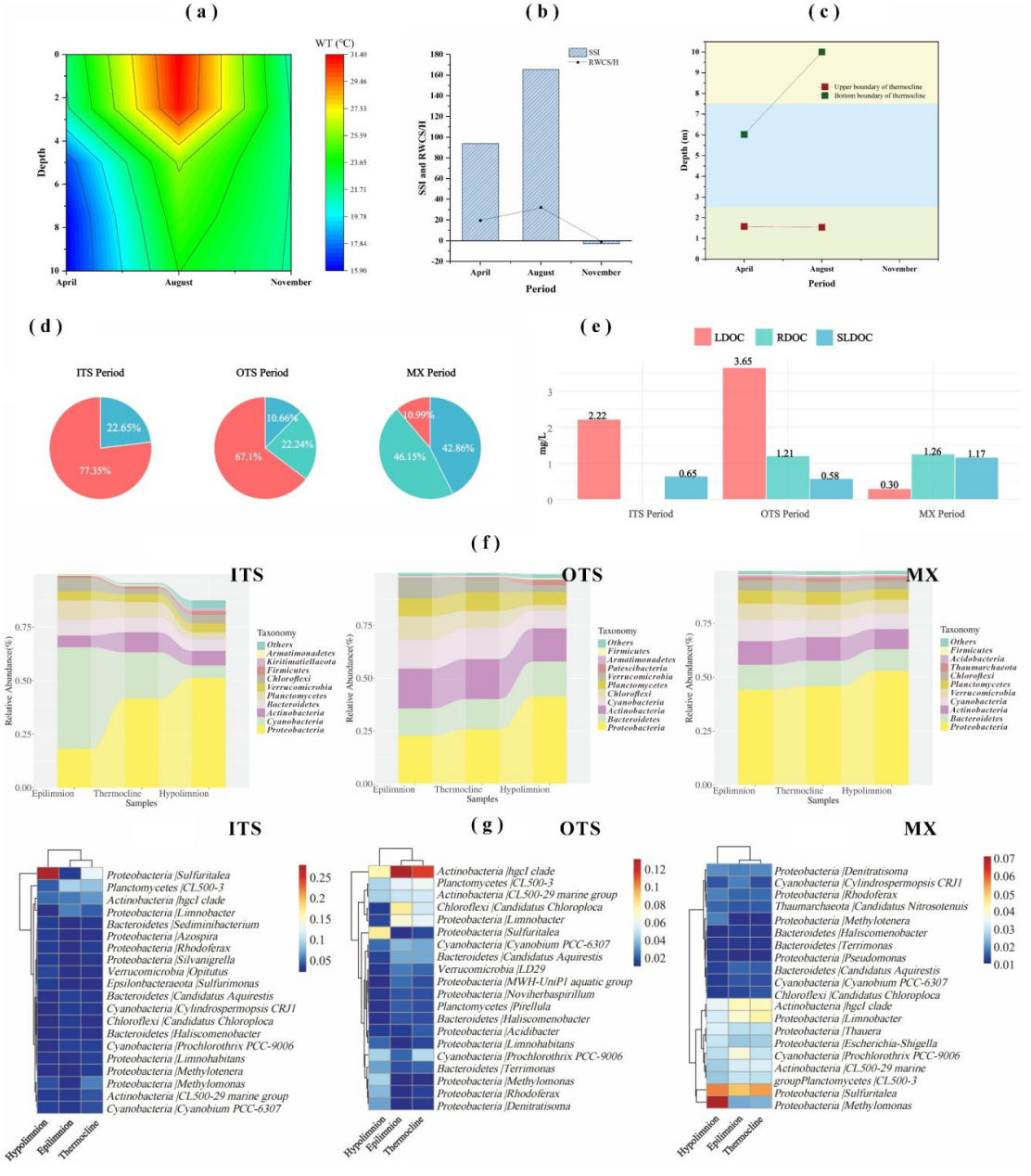

386

387 **Fig.2 Vertical water temperature profile in the DLD Reservoir during the study period (a),**

388 **temporal variations of SSI and RWCS/H index(negative values of RWCS/H were observed**

389 **during the late mixing period, indicating a temporary density inversion that facilitates rapid**

https://doi.org/10.5194/egusphere-2026-4596
Preprint. Discussion started: 24 August 2026

vertical convective mixing) (b), depths of the upper and lower boundaries of the thermocline (c); the proportions (d) and concentrations (e) of each component of DOM in the water bodies during ITS, OTS, and MX periods; and the top 10 (f) and top 20 (g) bacterial genera and species levels in the water body of the DLD reservoir during the ITS, OTS and MX periods, respectively.

3.2 DOM component characteristics

Parallel factor analysis distinguished five DOC categories across the water-column profiles during the ITS, OTS, and MX phases of the DLD Reservoir. Overall, the resolved fractions comprised three LDOC components, one SLDOC component, and one RDOC component **(classification criteria are provided in Text S1)**. Under ITS conditions, PARAFAC resolved C1, C2, and C3, which were assigned to the LDOC and SLDOC fractions. With the development of OTS, the component profile expanded to C1, C3, C4, and C5, encompassing all three fractions of LDOC, SLDOC, and RDOC. Following transition to the MX phase, C1, C2, and C4 were detected and corresponded to SLDOC, LDOC, and RDOC, respectively **(Text S2)**.

Research has shown that DOC constitutes a substantial proportion of DOM, often accounting for approximately 50% or more of its composition **(Moody and Worrall, 2017)**. Therefore, in this study, DOC concentration was used as a proxy for DOM concentration. Based on the measured DOC concentrations (mg/L) at each sampling site in the DLD Reservoir and the fluorescence intensity contribution rates (%) of various DOM components, the concentrations of RDOC and LDOC (mg/L) at each sampling site were calculated using the equation: RDOC/LDOC (%) × DOC

https://doi.org/10.5194/egusphere-2026-4596
Preprint. Discussion started: 24 August 2026

(mg/L) = RDOC/LDOC (mg/L).

Based on the fluorescence component contribution ratios and DOC concentration calculations, both Thermal stratification (ITS and OTS) periods exhibited higher fluorescence intensity contributions and concentrations of LDOC compared to the MX period **(Fig.2 (d) and (e))**. During the ITS period, LDOC and SLDOC accounted for approximately 76.9% and 23.1% of the total fluorescence intensity, with corresponding concentrations of 2.22 mg/L and 0.65 mg/L, respectively. In the OTS period, LDOC, SLDOC, and RDOC contributed 64.7%, 12.3%, and 23.0% of the total fluorescence intensity, with concentrations of 3.65 mg/L, 0.58 mg/L, and 1.21 mg/L, respectively. During the MX period, the fluorescence intensity contributions of LDOC, SLDOC, and RDOC in the DLD Reservoir were 11.2%, 42.6%, and 46.2%, respectively. Based on the concentration calculation formula, the average concentrations of these DOC categories were 0.30 mg/L, 1.17 mg/L, and 1.26 mg/L, respectively. Spatial variations in DOM component concentrations across the different periods are provided in **Text S2 and Fig. S3**.

3.3 Bacterial Community Structure and Interactions

3.3.1 Spatial and Temporal Distribution Pattern of Bacteria

Amplicon sequencing of samples collected during the three thermal phases yielded 411,458 high-quality bacterial OTUs after quality control. Taxonomic assignment indicated that the bacterial assemblages primarily comprised *Proteobacteria*, *Cyanobacteria*, *Bacteroidetes*, and *Actinobacteria*. Together, these four most abundant phyla contributed approximately 50%-70% of the overall community. Clear temporal shifts in their relative contributions were observed among

https://doi.org/10.5194/egusphere-2026-4596
Preprint. Discussion started: 24 August 2026

the three phases **(Fig. 2f)**. Under ITS conditions, *Proteobacteria* contributed the largest fraction (38% ± 17%), followed by *Cyanobacteria* (24% ± 19%) and *Actinobacteria* (8% ± 3%). With the establishment of OTS, the relative contribution of *Proteobacteria* decreased to 31% ± 9%, whereas *Actinobacteria* and *Bacteroidetes* accounted for 18% ± 2% and 15% ± 4%, respectively; *Cyanobacteria* represented a comparatively smaller fraction of 12% ± 4%. Following the transition to MX conditions, *Proteobacteria* increased to 48% ± 8% of the bacterial assemblage, while *Bacteroidetes* and *Actinobacteria* contributed 11% ± 2% and 10% ± 2%, respectively. By comparison, the contribution of *Cyanobacteria* declined further to 8% ± 2%.

Analysis of genus-level bacterial composition revealed clear spatiotemporal heterogeneity in community distribution. During ITS, however, the proportional representation of individual bacterial genera varied only slightly among water layers. The most abundant genus in the hypolimnion was *Sulfuritalea* (*Proteobacteria*) (29% ± 7%), which also dominated the thermocline (12% ± 11%). In the epilimnion, the genus *CL500-3* (*Planctomycetes*) exhibited the highest relative abundance (8% ± 1%) **(Fig.2 (g))**. In the OTS period, greater variation in bacterial relative abundance was observed among water layers. The hgcI clade, affiliated with Actinobacteria, showed greater representation in the upper two layers, accounting for 12.9% ± 2.4% in the epilimnion and 10.4% ± 2.5% in the thermocline. In the hypolimnion, *Sulfuritalea* (*Proteobacteria*) remained the most dominant genus (7.4% ± 4.8%) **(Fig.2 (g))**. During the MX period, *Methylomonas* (*Proteobacteria*) reached its highest relative abundance in the hypolimnion (7.9% ± 0.9%), while its distribution was more uniform in the middle and surface layers. *Sulfuritalea* (*Proteobacteria*) showed the second-highest overall abundance (6.2% ± 1.0%) and maintained

https://doi.org/10.5194/egusphere-2026-4596
Preprint. Discussion started: 24 August 2026

relatively even distribution across all three water layers **(Fig.2 (g))**.

3.3.2 Distribution Characteristics of Keystone Taxa Regulate DOM Bioavailability

The ecological positions of bacterial OTUs within the reservoir association networks were evaluated across the three thermal phases using two node-level parameters: connectivity within individual modules (Zi) and connectivity across modules (Pi). According to these metrics, all nodes were assigned to one of four topological categories following previously established criteria **(Guimerà and Nunes Amaral, 2005; Ma et al., 2021) (Fig.3 (a)-(c)).** Network hubs occurred exclusively during OTS period, with two such nodes identified in this phase. Because Connectors, Module hubs, and Network hubs represent highly connected positions that contribute substantially to the structural integrity of microbial networks, taxa belonging to these three categories were regarded as keystone members. Across ITS, OTS, and MX, the corresponding networks contained 1, 4, and 8 Module hubs and 22, 10, and 3 Connectors, respectively, whereas Peripheral nodes numbered 329, 533, and 421 **(Table 1)**. Further information on the taxonomic composition and abundance of keystone members identified in the DLD Reservoir during each thermal period is provided in **Text S5** and **Table 1**.

https://doi.org/10.5194/egusphere-2026-4596
Preprint. Discussion started: 24 August 2026

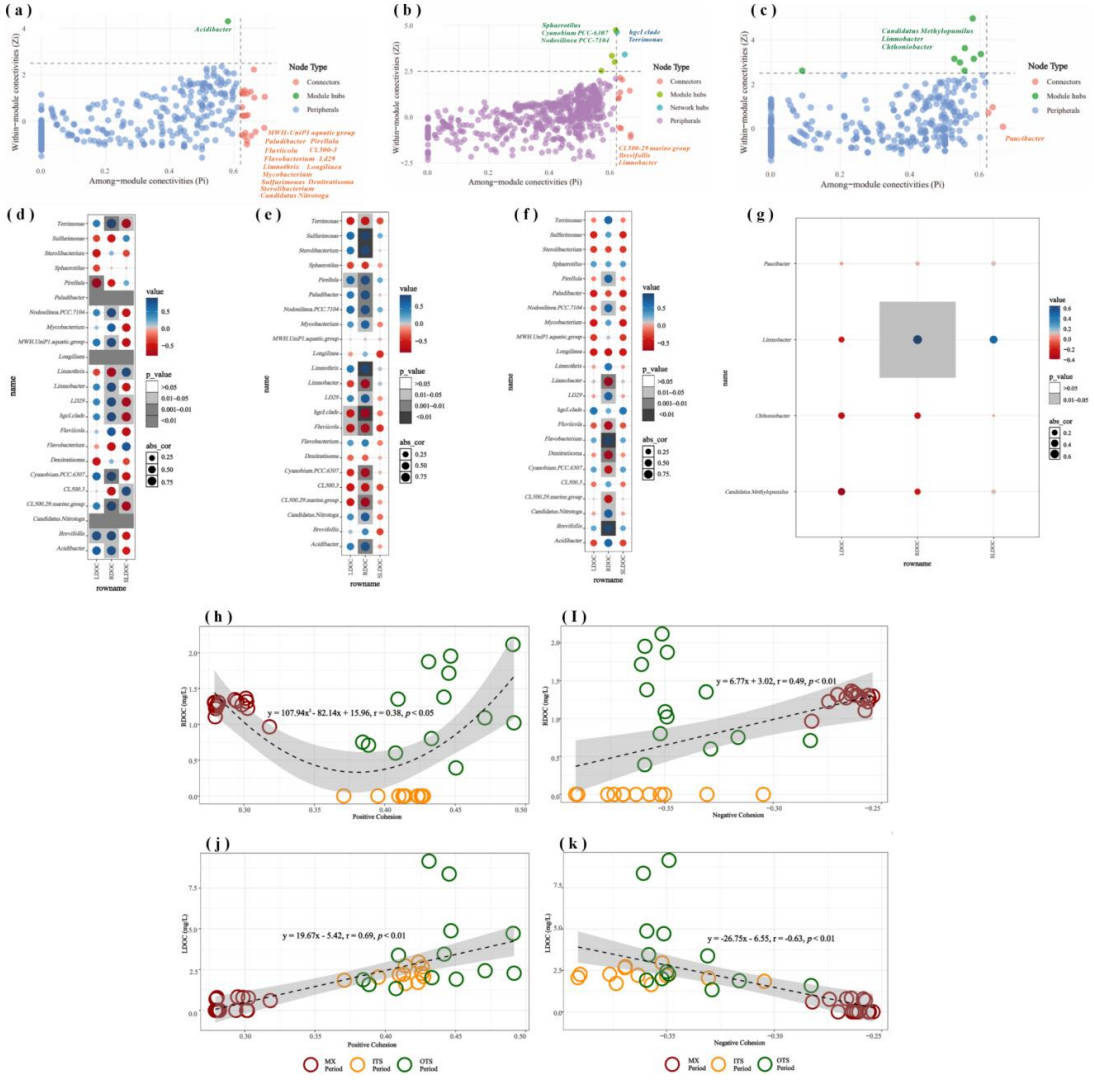

Fig.3 Node classification for identifying putative keystone taxa in the networks of the (a) ITS period, (b) OTS period, and (c) MX period. Each symbol represents an OTU derived from detailed modular analysis of the two networks. Categories include: Module hubs (nodes with high connectivity within their own module, defined as Zi > 2.5 and Pi < 0.62), Connectors (nodes with high connectivity between different modules, defined as Zi < 2.5 and Pi > 0.62),

https://doi.org/10.5194/egusphere-2026-4596
Preprint. Discussion started: 24 August 2026

475 **Network hubs (nodes with high connectivity across the entire network, defined as Zi > 2.5**
476 **and Pi > 0.62), and Peripherals (nodes with low connectivity both within and between**
477 **modules, defined as Zi < 2.5 and Pi < 0.62). Bacterial names in the figure correspond to the**
478 **genus-level taxonomy represented by each OTU node. Heatmap showing the Spearman**
479 **correlation between the relative abundance of bacterial genera in the key bacterial groups of**
480 **the water bodies and the concentrations of LDOC, SLDOC and RDOC during the thermal**
481 **stratification period (d), thermocline (e), bottom water layer (f), and mixed period (g).Linear**
482 **and non-linear regression analyses of positive ((h) and (j)) and negative ((i) and (k)) cohesion**
483 **with LDOC and RDOC of bacteria in DLD reservoir.**

484

485 **Table 1. Detailed phylogenetic relationships of Keystone taxa in the Zi-Pi diagram**

Networks	Node type	Number of OTUs	Phylum	Genus
Incabating thermal stractification period	Module hubs	1	*Proteobacteria* (1)	*Acidibacter* (1)
	Connectors	22	*Proteobacteria* (7)	*Paludibacter* (1),
			Bacteroidetes (4)	*Unclassified* (5),
			Planctomycetes (3)	*Fluviicola* (2),
			Firmicutes (2)	*Flavobacterium* (1),
			Cyanobacteria (1)	*Limnothrix* (1),
			Verrucomicrobia (1)	*Pirellula* (1), *CL 500-3* (2), *LD 29* (1),
			Hydrogenedentes (1)	*Longilinea* (1),
			Chloroflexi (1)	*Mycobacterium* (1),
			Actinobacteria (1)	*Sulfurimonas* (1),
			Epsilonbacteraeota	*Sterolibacterium* (1),

https://doi.org/10.5194/egusphere-2026-4596
Preprint. Discussion started: 24 August 2026

			(1)	*Denitratisoma* (1), *Candidatus Nitrotoga* (1) *Rubrivivax* (1)，*MWH-UniP1 aquatic group* (1)
Obvious thermal stratification period	Connectors	10	*Actinobacteria* (4) *Proteobacteria* (2) *Cyanobacteria* (1) *Bacteroidetes* (1) *Verrucomicrobia* (1) *Planctomycetes* (1)	*CL 500-29 marine group* (4), *Cyanobium PCC-6307* (1), *Brevifollis* (1), *Limnobacter* (1), *Unclassified* (3)
	Module hubs	4	*Cyanobacteria* (2) *Proteobacteria* (2)	*Cyanobium PCC-6307* (1), *Nodosilinea* (1), *Sphaero tilus* (1), *Unclassified* (1)
	Network hubs	2	*Actinobacteria* (1) *Bacteroidetes* (1)	*hgcI clade* (1) *Terrimonas* (1)
	Connectors	3	*Proteobacteria* (2) *Dependentiae* (1)	*Paucibacter* (1), *Unclassified* (2)
Mixing period	Module hubs	8	*Proteobacteria* (2) *Bacteroidetes* (3) *Verrucomicrobia* (2) *Actinobacteria* (1)	*Candidatus Methylopumilus* (1), *Limnobacter* (1), *Chthonibacter* (1), *Unclassified* (5)

Spearman coefficients were calculated to examine associations of genus-level bacterial abundances with LDOC, SLDOC, and RDOC concentrations among water layers under stratified conditions (TS, comprising ITS and OTS) and during MX in the DLD Reservoir. Because vertical thermal stratification disappeared under MX conditions, the entire water column was considered without further division into individual layers. The relationships linking keystone bacterial taxa to

https://doi.org/10.5194/egusphere-2026-4596
Preprint. Discussion started: 24 August 2026

RDOC and LDOC at different depths are presented in **Fig. 3(d-g)**.

Clear depth-dependent associations with RDOC emerged during OTS. Within the epilimnion, higher abundances of LD29, MWH-UniP1 aquatic group, *Acidibacter*, *Nodosilinea* PCC 7104, *Limnobacter*, and *hgcI clade* coincided significantly with elevated RDOC concentrations ($p < 0.05$). Even stronger positive associations were detected for *Terrimonas*, *Cyanobium PCC 6307*, and *CL500-29 marine group* ($p < 0.01$). In deeper hypolimnetic waters, RDOC formation was associated only with *LD29*, *Flavobacterium*, *Candidatus Nitrotoga*, *Pirellula*, *Brevifollis*, and *Nodosilinea*. After transition to MX conditions, *Limnobacter* was the sole genus exhibiting a positive relationship with RDOC ($p < 0.05$).

Associations involving LDOC differed markedly among vertical zones under stratified conditions. *Brevifollis* was the only keystone genus related to LDOC within the epilimnion. At thermocline depths, increasing abundances of *hgcI clade* and *Fluviicola* corresponded to significant decreases in LDOC, whereas *Pirellula* displayed the opposite pattern, with a significant positive association. No keystone taxon exhibited a statistically detectable relationship with LDOC either in the hypolimnion under TS conditions or throughout the unstratified water column during MX.

Relationships involving SLDOC were restricted to the epilimnion under thermal stratification. Greater representation of *CL500-3* and *Limnothrix* was associated with higher SLDOC concentrations ($p < 0.05$), whereas *LD29*, *CL500-29 marine group*, *hgcI clade*, and *Terrimonas* displayed inverse associations with SLDOC ($p < 0.05$). Taken together, the spatial and temporal patterns of these Spearman relationships suggest that keystone taxa are more closely associated

https://doi.org/10.5194/egusphere-2026-4596
Preprint. Discussion started: 24 August 2026

with processes governing RDOC production and persistence than with those responsible for LDOC and SLDOC generation and degradation in the aquatic environment.

3.3.3 Driving Effects of Bacterial Community Cohesion on DOM Bioavailability

Positive cohesion represents facilitative microbial interactions, while negative cohesion reflects competitive relationships **(Yuan et al., 2021; Herren and McMahon, 2017)**. The spatio-temporal variations in the average values of positive and negative bacterial cohesive values in the DLD reservoir are calculated as shown in **Table S2** and **Text S6**.

A regression analysis was conducted between the overall RDOC and LDOC concentrations in the water column of DLD Reservoir and the corresponding positive and negative cohesion values at each sampling point **(Fig.3 (h)-(k))**. As shown in **Fig. 3(h)**, a non-linear correlation was observed between bacterial positive cohesion and RDOC concentration ($p < 0.05$), with the scatter points forming a U-shaped pattern. On the left side of the U-shape, all sampling points within the 95% confidence interval were from the MX period, indicating that RDOC concentration decreased non-linearly with increasing positive cohesion during this period. On the right side of the U-shape, most sampling points from the OTS period fell within the 95% confidence interval, suggesting that RDOC levels increased with rising positive cohesion during this phase. In contrast to the linear relationships observed in **Fig. 3((i)-(k))**, the correlation between positive cohesion and RDOC **(Fig. 3(h))** was best characterized by a quadratic (U-shaped) model. This non-linearity reflects a functional shift in microbial facilitative interactions between hydrological periods. In the MX period, the negative correlation suggests that increased bacterial cooperation may be directed

https://doi.org/10.5194/egusphere-2026-4596
Preprint. Discussion started: 24 August 2026

toward carbon consumption under low-temperature, low-productivity conditions. Conversely, in the OTS period, positive cohesion appears to promote RDOC production via the MCP effect. This bimodal response distinguishes RDOC accumulation from the consistent linear trends observed for LDOC **(Fig. 3(j), (k))**.

By comparison, positive cohesion increased linearly with LDOC concentration ($r = 0.69$, $p < 0.01$) **(Fig. 3(j))**. A similar increasing trend was observed between bacterial negative cohesion and RDOC concentration ($r = 0.49$, $p < 0.01$) **(Fig. 3(i))**, while the relationship between negative cohesion and LDOC was inverse ($r = -0.63$, $p < 0.01$) **(Fig. 3(k))**. Collectively, these patterns suggest that facilitative bacterial associations in the DLD Reservoir favored LDOC formation, with greater positive cohesion corresponding to enhanced LDOC production. In contrast, competitive and inhibitory associations appeared to constrain LDOC formation and potentially accelerate its utilization, while simultaneously favoring RDOC production and retention.

3.3.4 Regulation of DOM Bioavailability by Environmental Factors in Stratified Water Columns

Across the TS phases, encompassing both ITS and OTS, significant associations between environmental variables and DOM components were detected in the epilimnion of the DLD Reservoir. SLDOC concentrations increased significantly with DO, TN, and FI ($p < 0.05$), whereas an inverse relationship was detected between positive cohesion and SLDOC ($p < 0.05$) **(Fig. 4(a))**. LDOC was positively associated with pH but varied inversely with pCO_2 ($p < 0.05$). For RDOC, higher concentrations coincided significantly with increases in TP and the Simpson index ($p < 0.05$),

https://doi.org/10.5194/egusphere-2026-4596
Preprint. Discussion started: 24 August 2026

while HCO_3^- showed the opposite relationship with RDOC levels ($p < 0.05$).

Within the thermocline **(Fig. 4(b))**, LDOC increased significantly with both WT and FI ($p < 0.05$). For RDOC, higher levels were significantly associated with WT, the Simpson index, and HIX, while an inverse association was detected with FI ($p < 0.05$).

Within the hypolimnion **(Fig. 4(c))**, LDOC was significantly associated with fewer environmental parameters, with positive cohesion being the only variable showing a positive relationship ($p < 0.05$). SLDOC likewise increased significantly with positive cohesion ($p < 0.05$). At the same depth, higher RDOC concentrations were significantly associated with elevated HCO_3^-, WT, TP, and TN ($p < 0.05$).

Under MX conditions **(Fig. 4(d))**, LDOC varied inversely with the Simpson index ($p < 0.05$). Higher HCO_3^-, pCO_2, and HIX values were significantly associated with lower concentrations of both SLDOC and RDOC ($p < 0.05$), whereas increasing pH corresponded significantly to higher levels of these two DOM fractions ($p < 0.05$). For RDOC specifically, its concentration increased significantly in association with DO, Chl-a, δ^{13}C-DIC, and the β:α ratio ($p < 0.05$).

https://doi.org/10.5194/egusphere-2026-4596
Preprint. Discussion started: 24 August 2026

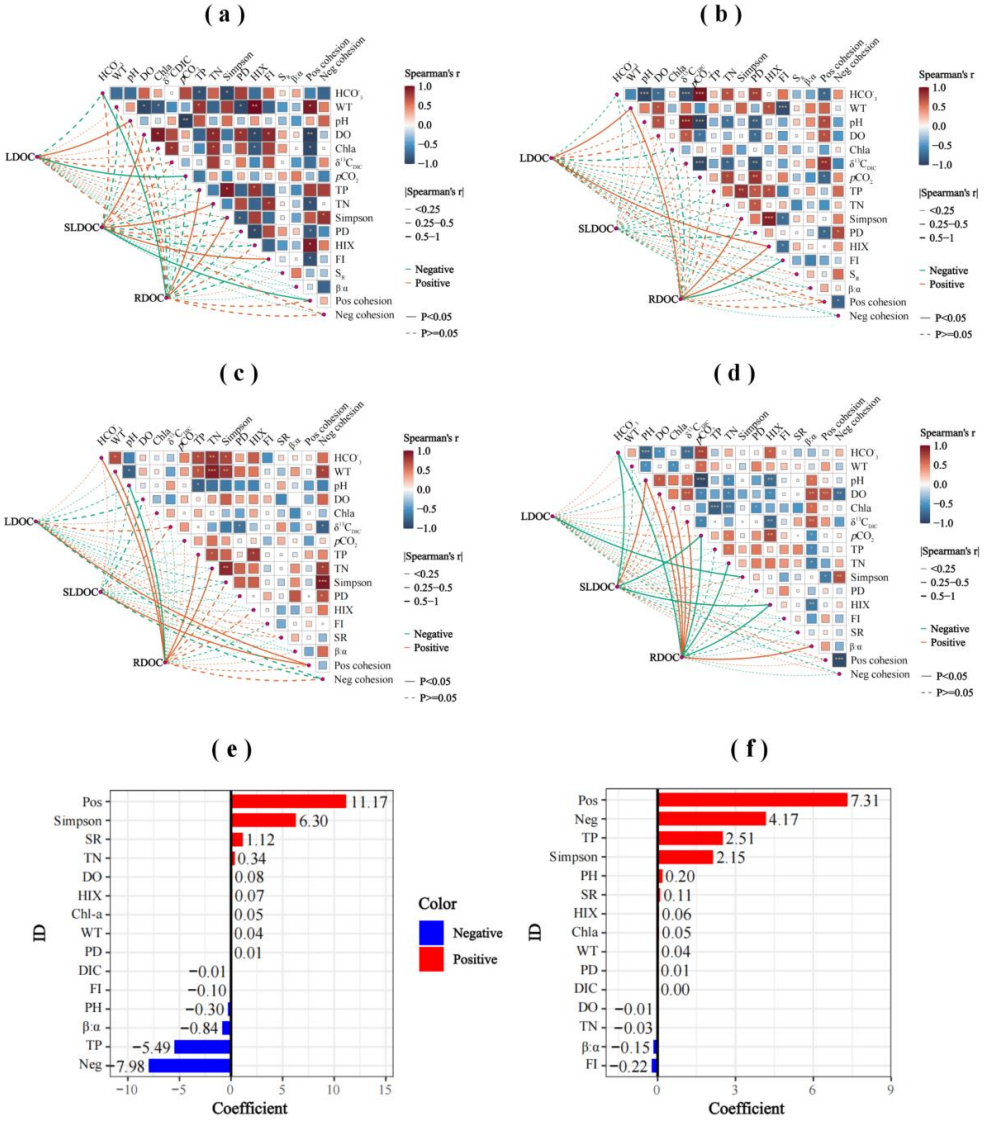

Fig.4 (a-d) Heatmaps of Spearman correlation coefficients from Mantel tests illustrating relationships among DOM, bacterial positive/negative cohesion, hydrochemical parameters, and spectral indices in DLD Reservoir: (a) epilimnion during TS periods, (b) thermocline during TS periods, (c) hypolimnion during TS periods, and (d) MX period (*p < 0.05, **p < 0.01, ***p < 0.001). (e-f) Bayesian linear regression analyses of environmental and spectral

https://doi.org/10.5194/egusphere-2026-4596
Preprint. Discussion started: 24 August 2026

indicators with (e) LDOC and (f) RDOC concentrations (red indicates positive coefficients, blue indicates negative coefficients; R^2 values for the models are 0.530 and 0.655, respectively).

Furthermore, as shown in **Fig. 4**, bacterial cohesion exhibited spatiotemporal correlations with environmental factors. In the epilimnion of the TS periods, positive cohesion correlated positively with WT and HIX, but negatively with DO, Chl-a, TN, PD, and FI. In the thermocline, it was positively linked to pH, DO, and $\delta^{13}C_{DIC}$, and negatively to HCO_3^-, pCO_2, and PD. In the hypolimnion, only negative cohesion showed significant correlations. During the MX period, DO strongly promoted positive cohesion but suppressed negative cohesion, while the Simpson index showed the opposite pattern.

Bayesian linear regression revealed distinct predictive effects on LDOC and RDOC **(Fig.4 (e) and (f))**. For LDOC, positive cohesion and the Simpson index were promotive predictors, while negative cohesion and TP were inhibitory. Bacterial activities and alkalinity (represented by alpha diversity and pH in **Fig.4 (e)**) exhibited inhibitory predictive effects on LDOC concentration—that is, higher values of these indicators predicted lower LDOC levels. In contrast, Chl-a showed a slight promotive predictive effect on LDOC, with higher values predicting increased LDOC concentration. For RDOC, positive cohesion, negative cohesion, and TP consistently exhibited promotive effects, while FI and the β:α ratio showed slight inhibition. Overall, cohesion metrics, nutrient status, and microbial alpha diversity dominated DOM bioavailability.

4. Discussion

4.1 Thermal Stratification Drives Spatiotemporal Differentiation in Microbial Interaction

https://doi.org/10.5194/egusphere-2026-4596
Preprint. Discussion started: 24 August 2026

Networks and RDOC Production

Thermal stratification provides the primary physical framework underlying temporal and vertical variations in reservoir microbial associations and RDOC formation. Suppression of water-column mixing during stratification generates pronounced vertical hydrochemical heterogeneity, with oxygen-rich conditions in surface waters and oxygen depletion at depth, which in turn promotes depth-specific organization of microbial assemblages **(Li et al., 2021; Jia et al., 2025)**. Within this stratified environment, keystone taxa assume central ecological roles by shaping the composition and functional attributes of microbial assemblages **(Banerjee et al., 2018)** and contributing directly to RDOC formation across different depths **(Shi et al., 2025)**. Evidence from network and correlation analyses **(Fig. S6)** further demonstrates close associations between keystone-taxon abundance and key hydrochemical variables, including water temperature, DO, and pH. Such relationships suggest that environmental gradients may regulate spatial patterns of RDOC formation through their effects on these ecologically influential taxa. These keystone taxa occupy central positions within microbial interaction networks and engage in multiple interaction pathways with both undefined genera and other keystone taxa (**Fig. 5**), further supporting their role in shaping the spatiotemporal patterns of RDOC production through complex microbial interactions. The manifestation of these complex interactions is most evident in the functional differentiation characteristics of microorganisms across water layers, where distinct functional segregation is evident **(Fig. 6)**.

In the epilimnion (**Fig. 6(a)**): *Limnothrix* is extensively involved in aerobic carbon transformation; *Flavobacterium* shows a positive correlation with photosynthetic functions, while

https://doi.org/10.5194/egusphere-2026-4596
Preprint. Discussion started: 24 August 2026

Mycobacterium exhibits a negative correlation; *Brevifollis* is negatively correlated with functions such as fermentation and methane oxidation, suggesting it may play an inhibitory role in the carbon cycle. *CL500-3* and *Fluviicola* exhibit opposite correlations in xylan and chitin degradation, reflecting niche differentiation in complex organic matter degradation. In the thermocline (**Fig. 6(b)**), chloroplast-related functions, chitin degradation, and anaerobic photoautotrophy show significant correlations with numerous bacterial groups, demonstrating strong functional coupling between groups. In the hypolimnion (**Fig. 6(c)**), photosynthesis-related functions showed significant positive correlations with *Terrimonas* and *Acidibacter*; xylan degradation was negatively correlated with multiple bacterial groups, while cellulose and chitin degradation were positively correlated with specific groups. In methane oxidation, *Fluviicola* showed negative correlations with oxidative functions, whereas *Brevifollis* and *Flavobacterium* often exhibited positive correlations. In methane production, hydrogenotrophic methanogenesis showed significant positive correlations with Bacillus longus and *Limnobacter*. During the Mixing period (**Fig. 6(d)**), *Candidatus Methylopumilus* and *Chthoniobacter* correlated positively with carbon degradation and methane oxidation, while *Limnobacter* correlated negatively with nearly all metabolic functions, suggesting that its increased abundance may be accompanied by decreased functional activity.

This overarching functional segregation provides the ecological template upon which carbon transformation functions are dominated by distinct keystone taxa across different periods and layers. During the ITS period, *Fluviicola*, acting as a Connector in the co-occurrence network, indirectly influenced RDOC formation through heterotrophic metabolism and interspecies interactions.

https://doi.org/10.5194/egusphere-2026-4596
Preprint. Discussion started: 24 August 2026

Studies indicate that *Fluviicola* is ubiquitously distributed in freshwater environments, where its heterotrophic metabolic activity may indirectly modulate aquatic carbon cycling. Moreover, synergistic interaction with *Fluviicola* and *Polynucleobacter* are implicated in the RDOC formation and persistence of RDOC **(Shi et al., 2025)**. In the OTS period, the Cyanobacteria *Nodosilinea PCC-7104* and *Cyanobium PCC-6307* functioned as Module hubs, fixing CO_2 through photosynthesis and serving as primary producers of LDOC. These two Cyanobacterial taxa utilize photosynthesis and carbon concentration mechanisms (CCMs) to achieve carbon fixation. CCMs enable them to efficiently concentrate CO_2 under CO_2-limited conditions, thereby sustaining efficient carbon fixation catalyzed by ribulose-1,5-bisphosphate carboxylase/oxygenase (Rubisco) **(Kupriyanova et al., 2023)**. Their carbon fixation capacity is regulated by light intensity, as light energy drives the photosynthetic electron transport chain, influencing the production of ATP and NADPH, which in turn modulates carbon fixation efficiency **(Tu et al., 2023)**. These two bacterial taxa contribute substantially to carbon fixation within surface waters under thermally stratified conditions. Furthermore, in this period (**Fig. 5 and 6**), *hgcI clade* (Network hubs) and *CL500-29 marine group* (Connectors) not only connected different modules and nodes in the bacterial interaction network but also contributed to the transformation of both terrestrially derived and autochthonously produced LDOC, leveraging their carbon metabolic capabilities. The *CL500-29 marine group* is recognized as a core species in warm lakes **(Guo et al., 2023; Gómez-Consarnau et al., 2012)**, capable of degrading various carbon- and nitrogen-containing substrates **(Zhang et al., 2020)** and showing a positive correlation with rising water temperatures **(Guo et al., 2023)**, which aligns with our findings **(Fig. S6)**. The *hgcI clade* represents a prevalent bacterial lineage

https://doi.org/10.5194/egusphere-2026-4596
Preprint. Discussion started: 24 August 2026

across diverse freshwater ecosystems **(Newton et al., 2011)**. Members of this facultatively aerobic lineage are capable of light-supported metabolism **(Garcia et al., 2013; Ghylin et al., 2014)** and exhibit considerable capacity for the utilization of carbon compounds **(Ghylin et al., 2014)**. Meanwhile, *Terrimonas*, another Network hub during the OTS period, is closely associated with denitrification processes **(Yan et al., 2022)** and may indirectly regulate carbon metabolism by influencing the nitrogen cycle. During the MX period, when the water column of the DLD Reservoir was fully mixed, *Limnobacter* emerged as the sole Module hub in the co-occurrence network, and its relative abundance increased significantly with RDOC levels **(Fig. 3(d)-(g))**. This bacterium is affiliated with β-Proteobacteria and represents a typical thiosulfate oxidizer **(Xamxidin et al., 2022)**. Energy production can be sustained through sulfide oxidation, a process that facilitates electron-acceptor utilization by anaerobic microorganisms **(Bruser et al., 2000)** and provides favorable conditions for anaerobic phototrophs that exploit reducing equivalents derived from sulfide to support CO_2 fixation and anoxygenic phototrophic growth **(Bryant et al., 2011)**. In addition, its chemoautotrophic metabolism enables energy acquisition through oxidative transformation of reduced inorganic sulfur species, with oxidized nitrogen compounds serving as electron acceptors. This metabolic pathway establishes a biogeochemical linkage among sulfur oxidation, carbon turnover, and nitrogen transformation **(Hu et al., 2018)**. This explains why, during the MX period when DIC concentrations were the highest, *Limnobacter*—as the only keystone taxa significantly positively correlated with RDOC concentration **(Fig. 3(g))** — played a critical role in RDOC production by directly utilizing inorganic carbon sources and fixing CO_2 to synthesize organic carbon.

https://doi.org/10.5194/egusphere-2026-4596
Preprint. Discussion started: 24 August 2026

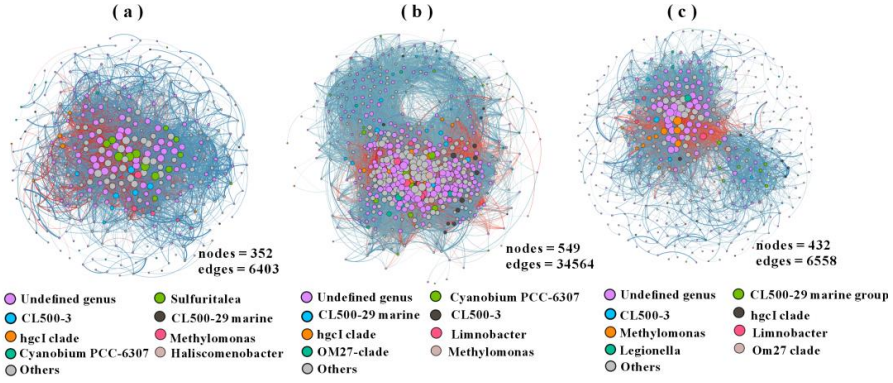

679

680 **Fig. 5. Genus-level bacterial association networks in the DLD Reservoir under (a) ITS, (b)**
681 **OTS, and (c) MX conditions. Red and blue links denote negative and positive associations,**
682 **respectively. "Nodes" refers to the total number of taxa included in each network, whereas**
683 **"Edges" denotes the total number of connections. Node size reflects the relative**
684 **representation of each bacterial genus within the community.**

685

https://doi.org/10.5194/egusphere-2026-4596
Preprint. Discussion started: 24 August 2026

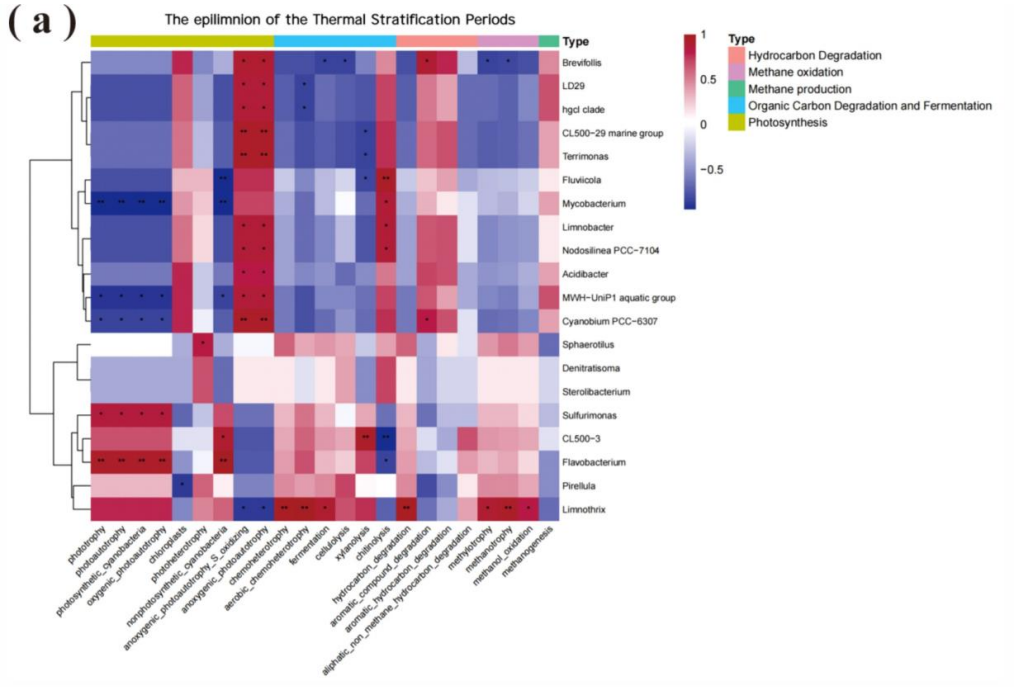

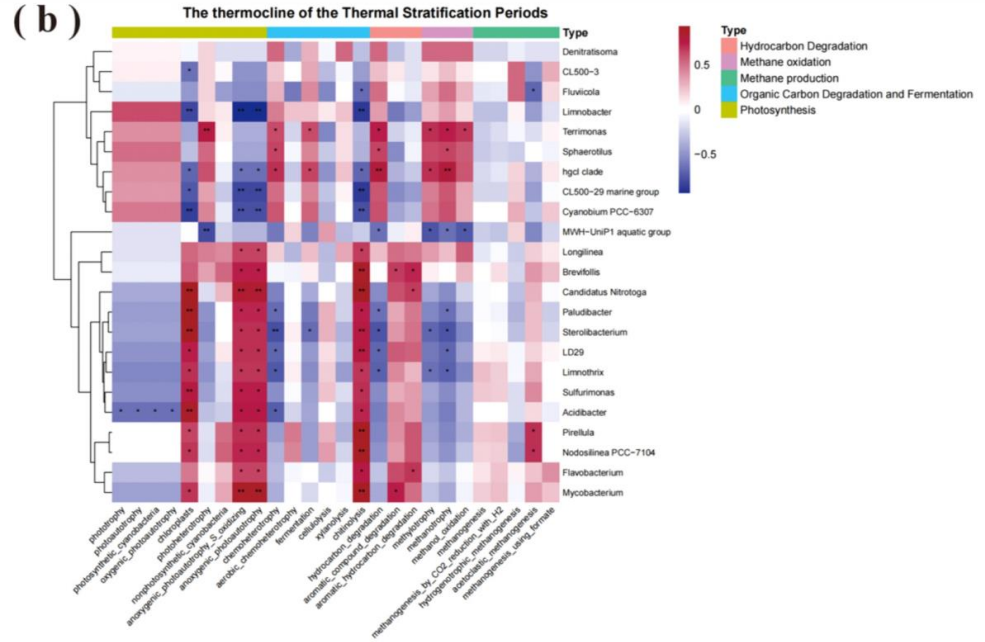

686

687

https://doi.org/10.5194/egusphere-2026-4596
Preprint. Discussion started: 24 August 2026

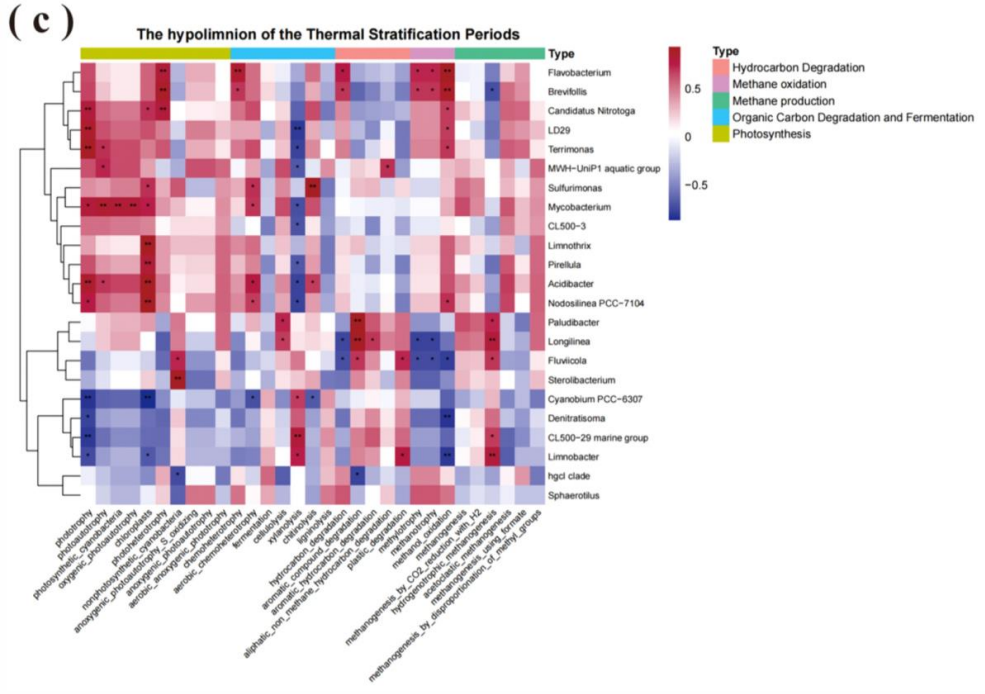

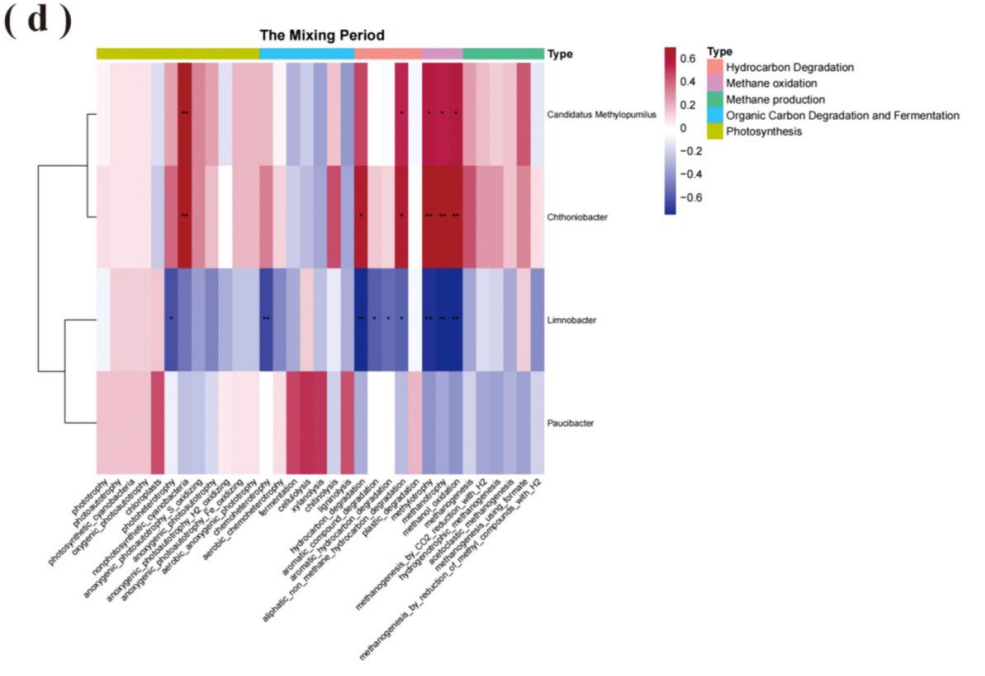

688

https://doi.org/10.5194/egusphere-2026-4596
Preprint. Discussion started: 24 August 2026

Fig. 6 Spearman correlation analysis of relative abundance and functional prediction of key taxa during the thermal stratification periods in the epilimnion (a), thermocline (b), hypolimnion (c), and Mixing period (d).

4.2 Bacterial Cohesion Reflects the MCP Mechanism

The succession of thermal stratification drives shifts in key environmental parameter. These environmental changes subsequently determine the balance between positive and negative bacterial cohesion across different water layers. Ultimately, this shift in microbial interaction patterns regulates the efficiency of the MCP and the resulting production of RDOC.

During ITS, enhanced light availability together with elevated water temperature favors phytoplankton proliferation, leading to substantial inputs of readily bioavailable DOM, within which carbohydrates and amino acids occur in relatively high proportions **(Meon and Kirchman, 2001; Amon et al., 2001)**. The resulting organic matter supplies heterotrophic bacteria with readily accessible carbon resources **(Wen et al., 2022)** , creating favorable conditions for facilitative associations among bacterial taxa and consequently enhancing microbial carbon pump (MCP) activity. Within these microbial networks, certain bacterial taxa may facilitate the proliferation of neighboring microorganisms or aquatic vegetation by producing various bioactive substances, such as B_{12} and other vitamins, extracellular enzymes, and compounds that promote growth **(Hu et al., 2025)**. Such biological exchanges can enhance LDOC supply while simultaneously reinforcing positive interspecific associations, thereby providing additional support for MCP-mediated carbon transformation. Consequently, the rise in positive cohesion during this period is accompanied by

https://doi.org/10.5194/egusphere-2026-4596
Preprint. Discussion started: 24 August 2026

an increase in RDOC concentration **(Fig.3(h))**. Studies have shown that algal–bacterial interactions further enhance RDOC production: algae provide dimethylsulfoniopropionate (DMSP) as a carbon source for bacteria, while bacteria reciprocate with vitamin B_{12}, enhancing algal photosynthetic carbon fixation and LDOC secretion. Through the MCP effect, approximately 20% of the biomass can be transformed into persistent RDOC, and horizontal gene transfer of sulfur metabolism genes also contributes to stabilizing algal-derived organic carbon **(Hu et al., 2025)**. As a result, LDOC concentration exhibits a linear increase with rising positive cohesion **(Fig.3(j))**. However, in environments with high bacterial diversity and intensified resource competition, the struggle for oxygen and organic matter leads to increased LDOC consumption. Under these conditions, LDOC decreases with increasing negative cohesion, while RDOC increases **(Fig.3(i) and (k))**, indicating that competitive negative cohesion also contributes to MCP-mediated carbon accumulation.

The scenario during the MX period reflects a legacy of the preceding thermal cycle, triggered by the complete water column overturn that redistributes dissolved organic matter. Although RDOC concentrations remain relatively high due to this vertical mixing, they represent a complex mixture: while allochthonous humic-like components persist, a significant portion is derived from the autochthonous RDOC that was efficiently generated and accumulated during the thermal stratification cycle (formation—stabilization—decline) through the DIC-enhanced MCP mechanism. Bacterial degradation capacity is reduced at lower temperatures, resulting in lower carbon conversion efficiency, and positive cohesion shows an inverse relationship with RDOC **(Fig.3 (h))**. The weakening of thermal stratification **(Hasan et al., 2013)** facilitates the sedimentation of POC thereby constraining bacterial transformation and RDOC formation. Although bacteria

https://doi.org/10.5194/egusphere-2026-4596
Preprint. Discussion started: 24 August 2026

731 increase cohesion to share limited resources under these conditions, the overall MCP effect remains
732 relatively weak.

733 In aquatic environments, both DO and bacterial diversity jointly regulate the type of cohesion
734 and the pathway of the MCP. High DO generally promotes the complexity of microbial networks
735 and facilitative interactions **(Hu et al., 2023)**, and stimulates the synthesis of extracellular
736 polymeric substances (EPS), enhancing bacterial aggregation **(Bowen et al., 2018)**. However, our
737 results revealed an inverse relationship between epilimnetic DO and positive cohesion, potentially
738 attributable to intensified resource competition under conditions of high bacterial diversity **(Fig.4**
739 **(a))**. In the thermocline, the uneven vertical distribution of DO correlate positively with positive
740 cohesion and negatively with negative cohesion. Within the oxygen-depleted hypolimnion, intense
741 competition for oxygen occurred, while negative cohesion declined as bacterial diversity increased.
742 Following the transition to MX conditions, the homogenization of DO throughout the water column
743 alleviated competitive pressure and favored cooperative interactions and metabolic activity among
744 aerobic bacteria **(Yue et al., 2022; Zhou et al., 2020)**. Accordingly, higher DO levels were
745 associated with greater positive cohesion but lower negative cohesion ($p < 0.05$). Similarly,
746 increased salinity has been shown to enhance competitive negative correlations **(Ji et al., 2019**),
747 further supporting the role of resource pressure in regulating the type of bacterial cohesion.

748 Given the relatively shallow water depth of the DLD Reservoir and the seasonal development
749 of hypolimnion under ITS and OTS conditions, sedimentary inputs of DOM cannot be excluded as
750 a potential source. Nevertheless, multiple observations from our dataset indicate that benthic
751 release is unlikely to dominate RDOC accumulation. First, analysis of the vertical distribution

https://doi.org/10.5194/egusphere-2026-4596
Preprint. Discussion started: 24 August 2026

revealed no significant RDOC enrichment in deeper waters compared with the surface layer, which deviates from the vertical trend anticipated under a sediment-dominated RDOC source scenario **(Fig. S3)**. Second, optical indices further discount a major benthic contribution: the HIX remained low in the hypolimnion, whereas sediment-derived DOM is typically characterized by high humic-like features **(Fig. S5)**. Furthermore, the FI shows no significant correlation with RDOC in most layers, and was even negatively correlated in the thermocline **(Fig. 4(a)-(d))**, suggesting that the RDOC pool does not predominantly mirror allochthonous-like signals from the sediment.

Most importantly, the relationship between RDOC and metabolic indicators supports a water-column origin. RDOC concentrations were not significantly associated with DO across the stratified layers, whereas higher RDOC levels coincided significantly with increasing DO under MX conditions **(Fig. 4(a)-(d))**. Such covariation under oxygenated conditions, rather than the inverse relationship anticipated from anaerobic sedimentary release, is consistent with microbial processing of autochthonous carbon. Furthermore, RDOC increased significantly in association with $\delta^{13}C_{DIC}$ under fully mixed conditions **(Fig. 4(d))**, suggesting a potential mechanistic connection mediated by microbial carbon fixation. The preferential uptake of $^{12}CO_2$ by chemoautotrophic taxa for biosynthesis causes a progressive ^{13}C-enrichment in the residual DIC pool. Concurrently, the enhanced carbon fixation flux produces substantial labile organic precursors. These precursors are subsequently channeled through the microbial food web and transformed into refractory compounds via the MCP. Therefore, the observed positive correlation is not a direct stoichiometric coupling, but rather a rate-coupling signature: higher in-situ CO_2 fixation rates simultaneously elevate both the $\delta^{13}C$ signal in the remaining DIC and the

https://doi.org/10.5194/egusphere-2026-4596
Preprint. Discussion started: 24 August 2026

accumulation of newly-formed RDOC, confirming that the RDOC pool originates primarily from water-column internal carbon processing rather than external inputs. Collectively, these results demonstrate that while sediment-water exchange is a physical reality in shallow systems, the RDOC dynamics in DLD Reservoir are fundamentally governed by the DIC-enhanced MCP within the water column rather than internal loading from the benthos.

4.3 Nutrient Imbalance-Driven Carbon Sequestration: Coupling Mechanisms Between BCP and MCP in Karst Reservoirs

In the carbon cycle of karst reservoirs, BCP initiates the primary production of endogenous organic carbon, whilst MCP is the key factor determining whether these carbon sources can be retained over the long term and converted into carbon sequestration. RDA analysis results **(Fig. 7)** indicate that during thermocline and mixing periods, environmental factors such as DIC, pH, WT and DO were significantly correlated with key microbial community structures ($R^2 > 0.3$, $p < 0.05$). This suggests that, within a karst weathering context, the cyclical evolution of reservoir thermocline structures shapes specific microbial community patterns by modulating the water chemistry. Concurrently, the persistent strong correlations between Chl-a, TN, TP and key microbial communities highlight the regulatory role of nutrient status on community structure. Driven by these environmental factors, the regulated microbial communities further alter the bioavailability of DOM via the MCP effect **(Fig. 3 (d)-(g))**.

https://doi.org/10.5194/egusphere-2026-4596
Preprint. Discussion started: 24 August 2026

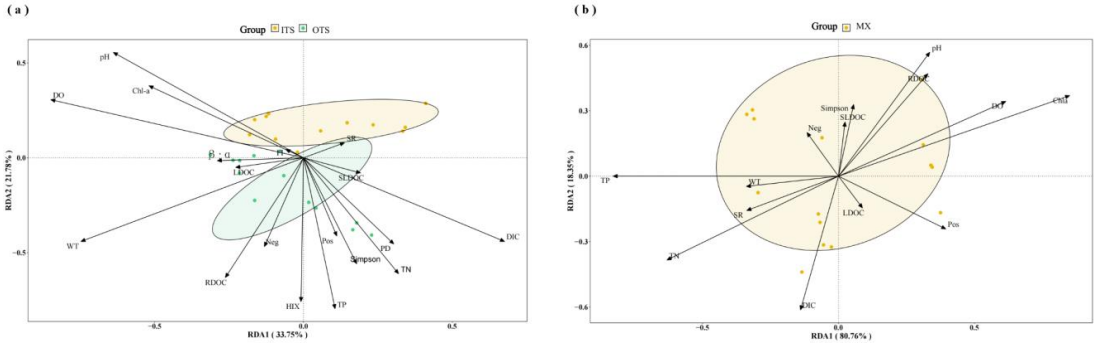

Fig. 7 RDA analysis using keystone taxa from the Thermal Stratification periods (a) and Mixing period (b) as response variables, with other indicators as predictor variables.

This study found that this transition from production to sequestration is strongly influenced by the unique geochemical environment of karst landscapes. Among these environmental filters, the carbonate-rich geochemical background exerts a unique regulatory effect on nutrient stoichiometry, which in turn acts as the primary switch for the BCP-MCP transition. A strongly significant quadratic relationship ($y = -1.7091 + 0.3601x - 0.0016x^2$, $R^2 = 0.395$, $p < 0.01$) is observed between Ca^{2+} concentration and the N:P ratio in **Fig.8(a)**, indicating a progressively accelerating positive response of N:P to increasing Ca^{2+} across the studied gradient. This nonlinear positive pattern likely reflects the enhanced removal of phosphate via calcium-phosphate precipitation (e.g., hydroxyapatite, HAP) under high-pH conditions **(Borkiewicz et al., 2010; Syers et al., 1973)**. This physicochemical barrier effectively reduces available phosphorus (SRP) in the water column, leading to a systemic stoichiometric imbalance in the C:P ratio **(Lu et al., 2023; Murphy and Hall, 1983)**. The significance of phosphorus is further supported by the Bayesian model **(Fig. 4(f))**, where TP is identified as a primary positive predictor of RDOC concentration. Although TP is essential for the initial carbon production through the BCP, its

https://doi.org/10.5194/egusphere-2026-4596
Preprint. Discussion started: 24 August 2026

positive correlation with RDOC indicates that in karst reservoirs, the total nutrient level does not reflect what is actually available for microbial use. Due to the geochemical immobilization of phosphorus, the bioavailable portion remains low even as the total nutrient pool increases, which maintains the high C:P ratios that are necessary for carbon to persist in the water column.

Under phosphorus-limited conditions, RDOC increased significantly along the C:P gradient, following a quadratic polynomial relationship ($y = 83.145 - 104.291x + 54.075x^2$, $p < 0.05$; **Fig. 8(b)**), with the magnitude of the RDOC response becoming progressively stronger toward higher C:P values. The underlying biological mechanism can be explained from the following two perspectives: first, according to the theory of ecometrics, microbial growth is strictly limited by nutrient ratios **(Sterner and Elser, 2002)**. Studies have shown that when phosphorus supply is insufficient to sustain ribosomal RNA and ATP synthesis **(Li et al., 2018; Schuhmacher et al., 2014)** , microorganisms are unable to effectively convert the high-throughput carbon source produced by BCP into biomass, resulting in a significant decline in carbon use efficiency (CUE) **(Li et al., 2025)**. In such cases, microorganisms are forced to release excess carbon in the form of EPS or secondary metabolites **(Zevin et al., 2015)**. These metabolites are often enriched in structurally intricate aromatic moieties and exhibit strong resistance to chemical degradation, as exemplified by humin-like substances. Their limited bioavailability restricts subsequent utilization by heterotrophic microorganisms, ultimately favoring the persistence and accumulation of RDOC in aquatic environments **(Jiao et al., 2010; Jiao et al., 2024)**. Furthermore, nutrient stress also inhibits extracellular enzyme activity, slowing down the rate of organic matter mineralization and accelerating its conversion into humus. The degradation of organic matter relies on extracellular

https://doi.org/10.5194/egusphere-2026-4596
Preprint. Discussion started: 24 August 2026

hydrolases secreted by microorganisms, and the synthesis of such enzymes itself consumes significant amounts of nitrogen and phosphorus. Under phosphorus-limiting conditions, microorganisms tend to downregulate the expression of energy-intensive enzymes to conserve resources **(Bilyera et al., 2021; Sun et al., 2023)**. This results in the failure of pre-existing active organic matter to be decomposed in a timely manner, causing it to persist in the water column for extended periods. Over long scales, these organic compounds undergo photochemical oxidation and repeated microbial reprocessing, transforming through molecular rearrangement into a reservoir of RDOC with more complex structures and greater biological resistance **(Liu et al., 2026; Obernosterer and Benner, 2004)**. In summary, the Ca-P co-precipitation effect, which is unique to karst reservoirs, amplifies phosphorus limitation in the water body. By reducing microbial carbon utilization efficiency and inhibiting enzymatic degradation, it synergistically drives the coupled transition from BCP to MCP. The higher the C:P ratio, the more pronounced this phosphorus-limitation-induced carbon reduction effect becomes, thereby reinforcing the function of karst reservoirs as regional carbon sinks.

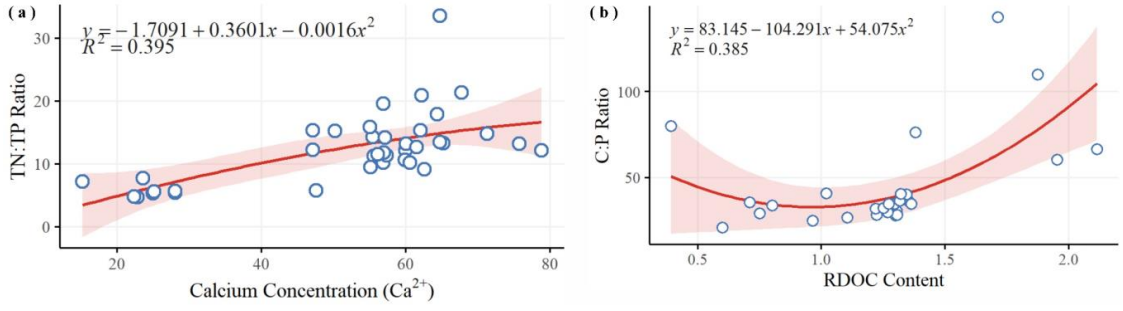

Fig. 8 Linear correlation analysis of calcium ion concentration with TN:TP (a), and linear correlation analysis of C:P in water bodies with RDOC concentration (b).

https://doi.org/10.5194/egusphere-2026-4596
Preprint. Discussion started: 24 August 2026

5. Conclusion

In summary, this research establishes a multi-dimensional framework to elucidate the mechanisms by which karst reservoirs function as effective regional carbon sinks. Central to this framework is the role of thermal stratification, which provides the structural foundation for carbon transformation. By restricting vertical mixing, stratification creates partitioned ecological niches where keystone bacterial taxa facilitate the conversion of labile organic matter into refractory forms; this accumulation of RDOC is independent of benthic inputs. This physical structure is further modulated by microbial dynamics, which regulate the efficiency of the MCP. The fluctuating balance between facilitative and competitive interactions across hydrological periods dictates whether organic carbon is remineralized or sequestered, with competitive interactions under environmental stress proving essential for the long-term persistence of the RDOC pool. Most significantly, the geochemical "Ca-P co-precipitation" effect acts as the primary catalyst for carbon sequestration. By depleting bioavailable phosphorus, this process imposes a severe stoichiometric constraint that decouples carbon uptake from biomass synthesis. This nutrient-limitation forcing inhibits enzymatic mineralization and promote microbial metabolism, effectively shunting excess carbon into stable, chemically complex RDOC.

Ultimately, the synergy between geochemical nutrient-locking and microbial processing intensifies the coupling of the BCP and MCP. This study underscores that the carbon sink capacity of karst reservoirs is fundamentally enhanced by their unique alkaline-calcium geochemistry, which facilitates carbon sequestration by imposing severe restrictions on phosphorus

https://doi.org/10.5194/egusphere-2026-4596
Preprint. Discussion started: 24 August 2026

bioavailability for the microbial community. This integrated mechanism provides a robust scientific foundation for incorporating karst-specific aquatic processes into global carbon budget models.

Author Contribution

Yikun Jia：Conceptualization, Methodology, Formal analysis, Software，Data Curation ,Writing - Original Draft, Writing - Review & Editing. **Junbing Pu**：Conceptualization, Methodology, Validation, Resources, Writing - Review & Original drafting, Writing - Review & Editing, Project administration. **Zaihua Liu:** Conceptualization, Methodology, Resources, Writing - Review & Editing, Writing - Ori. **Qiufang He**：Resources, Writing - Review & Editing, Writing – Original Drafting, Project administration. **Xinlu Su**：Formal analysis, Data Curation, Software. **Tao Zhang**：Resources, Writing - Review & Editing, Writing - Original Drafting, Project administration. **Jianhong Li:** Resources, Data Curation, Writing - Review & Editing, Project administration. **Sibo Zeng:** Resources, Data Curation, Writing - Review & Editing, Project administration.

Conflict of Interest

The authors declare no conflicts of interest relevant to this study

Acknowledgements

This study was supported by the National Natural Science Foundation of China (NO. 42577087), the National Special Support Plan for High-Level Talent to Junbing Pu (Young Talent Plan, 2022), the Project of Young Top Talents of the Bowang Scholars Programme of Chongqing

https://doi.org/10.5194/egusphere-2026-4596
Preprint. Discussion started: 24 August 2026

Normal University (NO. BWQB2023016), and the Science and Technology Research Project of Chongqing Education Commission (NO. KJQN202300502).

Data Availability Statement

The microbial data, water chemical indicators, and the code used to analyze the relationship between them are available in a figShare repository at **Jia (2025)** https://doi.org/10.6084/m9.figshare.30855587. The code can also be found at the Github link (https://github.com/YikunJia/-/releases/tag/MCP). All data were plotted using Origian 2021, MATLAB, Arcgis 10.8 and R 4.4.3. The DOM analysis method: Parallel factor analysis was plotted using the MATLAB software, and the source code was referenced from **Colin (2008)** https://doi.org/10.4319/lom.2008.6.572.

References

Amon R. M. W., Fitznar H.-P., Benner R., 2001. Linkages among the bioreactivity, chemical composition, and diagenetic state of marine dissolved organic matter. Limnology and Oceanography. 46 (2): 287-297.

Arnemann J. 16S-rDNA-Sequenzierung, Lexikon der Medizinischen Laboratoriumsdiagnostik, Chapter 3636-1: Chapter 3636-3631.

Banerjee S., Schlaeppi K., van der Heijden M. G. A., 2018. Keystone taxa as drivers of microbiome structure and functioning. Nature Reviews Microbiology. 16 (9): 567-576.

Bao Q., Liu Z., Zhao M., Hu Y., Li D., Han C., Zeng C., Chen B., Wei Y., Ma S., Wu Y., Zhang Y., 2022. Role of carbon and nutrient exports from different land uses in the aquatic carbon sequestration and eutrophication process. Sci Total Environ. 813: 151917.

Bilyera N., Dippold M. A., Bleicher J., Maranguit D., Kuzyakov Y., Blagodatskaya E., 2021. Microbial tradeoffs in internal and external use of resources regulated by phosphorus and carbon availability. European Journal of Soil Biology. 106: 103353.

Borkiewicz O., Rakovan J., Cahill C. L., 2010. Time-resolved in situ studies of apatite formation in aqueous solutions. American Mineralogist. 95 (8-9): 1224-1236.

https://doi.org/10.5194/egusphere-2026-4596
Preprint. Discussion started: 24 August 2026

Bouvy M., Arfi R., Cecchi P., Corbin D., Pagano M., Saint-Jean L., Thomas S., 1998. Trophic coupling between bacterial and phytoplanktonic compartments in shallow tropical reservoirs (Ivory Coast, West Africa). Aquatic Microbial Ecology. 15: 25-37.

Bowen W. H., Burne R. A., Wu H., Koo H., 2018. Oral Biofilms: Pathogens, Matrix, and Polymicrobial Interactions in Microenvironments. Trends in Microbiology. 26 (3): 229-242.

Bruser T., Lens P. N. L., Truper H. G., 2000. The biological sulfur cycle. In: Environmental Technologies to Treat Sulfur Pollution / P.N.L. Lens and L.W. Hulshoff Pol. - London : IWA Publishing, 2000. - ISBN 1900222094.

Bryant D. A., Gregersen L. H., Frigaard N. U., 2011. Mechanisms and Evolution of Oxidative Sulfur Metabolism in Green Sulfur Bacteria. Frontiers in Microbiology. 2: 1-14.

Caballero M., Waters M. N., Amezcua M., Ruiz-Fernández A. C., Sigala I., Alcocer J., 2025. Recent human-induced ecological changes in a Neotropical karst lake of southern Mexico. CATENA. 256: 109119.

Chen L., Tan L., Zhao M., Sinha A., Wang T., Gao Y., 2023. Karst carbon sink processes and effects: A review. Quaternary International. 652: 63-73.

Friedlingstein P., Jones M. W., O'Sullivan M., etal., 2021. Global Carbon Budget 2021. Earth System Science Data. 14 (4): 1917-2005.

Friedlingstein P., O'Sullivan M., Jones M. W., etal., 2022. Global Carbon Budget 2022. Earth System Science Data. 14 (11): 4811-4900.

Friedlingstein P., O'Sullivan M., Jones M. W., etal., 2023. Global Carbon Budget 2023. Earth Syst. Sci. 15 (12): 5301–5369.

Garcia S. L., McMahon K. D., Martinez-Garcia M., Srivastava A., Sczyrba A., Stepanauskas R., Grossart H.-P., Woyke T., Warnecke F., 2013. Metabolic potential of a single cell belonging to one of the most abundant lineages in freshwater bacterioplankton. The ISME Journal. 7 (1): 137-147.

Ghylin T. W., Garcia S. L., Moya F., Oyserman B. O., Schwientek P., Forest K. T., Mutschler J., Dwulit-Smith J., Chan L. K., Martinez Garcia M., Sczyrba A., Stepanauskas R., Grossart H. P., Woyke T., Warnecke F., Malmstrom R., Bertilsson S., McMahon K. D., 2014. Comparative single-cell genomics reveals potential ecological niches for the freshwater acI Actinobacteria lineage. The ISME Journal. 8 (12): 2503-2516.

Goldscheider N., Drew D., (Eds.) Methods in karst hydrogeology, IAH: International Contributions to Hydrogeology, 26 (1st ed.). CRC Press. https://doi.org/10.1201/9781482266023,

Gómez-Consarnau L., Lindh M. V., Gasol J. M., Pinhassi J., 2012. Structuring of bacterioplankton communities by specific dissolved organic carbon compounds. Environmental Microbiology. 14 (9): 2361-2378.

Guimerà R., Nunes Amaral L. A., 2005. Functional cartography of complex metabolic networks. Nature. 433 (7028): 895-900.

Guo Y., Gu S., Wu K., Tanentzap A. J., Yu J., Liu X., Li Q., He P., Qiu D., Deng Y., Wang P., Wu Z., Zhou Q., 2023. Temperature-mediated microbial carbon utilization in China's lakes. Global Change Biology. 29 (17): 5044-5061.

Harris N. L., Gibbs D. A., Baccini A., Birdsey R. A., de Bruin S., Farina M., Fatoyinbo L., Hansen M. C., Herold M., Houghton R. A., Potapov P. V., Suarez D. R., Roman-Cuesta R. M., Saatchi S.

https://doi.org/10.5194/egusphere-2026-4596
Preprint. Discussion started: 24 August 2026

S., Slay C. M., Turubanova S. A., Tyukavina A., 2021. Global maps of twenty-first century forest carbon fluxes. Nature Climate Change. 11 (3): 234-240.
Hasan K., Alam K., Saidul Azam Chowdhury M., 2013. The Use of an Aeration System to Prevent Thermal Stratification of Water Bodies: Pond, Lake and Water Supply Reservoir. Applied Ecology and Environmental Sciences. 2 (1): 1-7.
He Q., Xiao Q., Fan J., Zhao H., Cao M., Zhang C., Jiang Y., 2022. The impact of heterotrophic bacteria on recalcitrant dissolved organic carbon formation in a typical karstic river. Science of The Total Environment. 815: 152576.
He R., Li Q., Yu S., Sun P., 2022. Variation of Recalcitrant Dissolved Organic Carbon in Karst Water under the Influence of Heterotrophic Bacteria and Its Environmental Controlling Factors. Acta Geoscientica Sinica. 43 (4): 438-448 (in Chinese).
Herren C. M., McMahon K. D., 2017. Cohesion: a method for quantifying the connectivity of microbial communities. ISME J. 11 (11): 2426-2438.
Houghton R. A., Nassikas A. A., 2017. Global and regional fluxes of carbon from land use and land cover change 1850–2015. Global Biogeochemical Cycles. 31 (3): 456-472.
Hu L., Ye Y., Li Y., Tan X., Liu X., Zhang T., Wang J., Du Z., Ye M., 2025. Bacteria–algae synergy in carbon sequestration: Molecular mechanisms, ecological dynamics, and biotechnological innovations. Biotechnology Advances. 83: 108655.
Hu M., Liu X., Ya T., Liu J., Zhang M., Wang X., 2023. Dissolved oxygen alters the microbial interactions of anammox consortia in PN/A process. Journal of Water Process Engineering. 53: 103697.
Hu X., Liu J., Liu H., Zhuang G., Xun L., 2018. Sulfur metabolism by marine heterotrophic bacteria involved in sulfur cycling in the ocean. Science China Earth Sciences. 61 (10): 1369-1378.
Ji M., Kong W., Yue L., Wang J., Deng Y., Zhu L., 2019. Salinity reduces bacterial diversity, but increases network complexity in Tibetan Plateau lakes. FEMS Microbiol Ecol. 95 (12): 1-10.
Jia Y., Su X., Zhang T., He Q., Li J., Pu J., 2025. High carbon fixation during thermal stratification period in a subtropical periodic stratified reservoir: Evidences from RDOC conversion efficiency driven by MCP. Water Research. 278: 123316.
Jia Y., Xi N., Li R., Fan J., Zhao W., Zhang T., Li J., Pu J., 2024. Aquatic photosynthetic carbon pump driven by periodic temperature variations affects dissolved inorganic carbon and hydrochemical characteristics in a groundwater-fed reservoir. Environmental Research. 252: 119041.
Jiao N., Herndl G. J., Hansell D. A., Benner R., Kattner G., Wilhelm S. W., Kirchman D. L., Weinbauer M. G., Luo T., Chen F., Azam F., 2010. Microbial production of recalcitrant dissolved organic matter: long-term carbon storage in the global ocean. Nature Reviews Microbiology. 8 (8): 593-599.
Jiao N., Luo T., Chen Q., Zhao Z., Xiao X., Liu J., Jian Z., Xie S., Thomas H., Herndl G. J., Benner R., Gonsior M., Chen F., Cai W.-J., Robinson C., 2024. The microbial carbon pump and climate change. Nature Reviews Microbiology. 22 (7): 408-419.
Kupriyanova E. V., Pronina N. A., Los D. A., 2023. Adapting from Low to High: An Update to CO_2-Concentrating Mechanisms of Cyanobacteria and Microalgae. Plants. 12 (7): 1569.

https://doi.org/10.5194/egusphere-2026-4596
Preprint. Discussion started: 24 August 2026

Li J., Pu J., Zhang T., 2021. Transport and transformation of dissolved inorganic carbon in a subtropical groundwater-fed reservoir, south China. Water Research. 209: 117905.
Li S., Cui Y., Moorhead D. L., Dijkstra F. A., Sun L., Xia Z., Gao Y., Ma Q., Yu W., 2025. Phosphorus limitation regulates the responses of microbial carbon metabolism to long-term combined additions of nitrogen and phosphorus in a cropland. Soil Biology and Biochemistry. 200: 109614.
Li S. H.-J., Li Z., Park J. O., King C. G., Rabinowitz J. D., Wingreen N. S., Gitai Z., 2018. Escherichia coli translation strategies differ across carbon, nitrogen and phosphorus limitation conditions. Nature Microbiology. 3 (8): 939-947.
Liu M., Zhang Y., Shi K., Melack J., Zhang Y., Zhou Y., Zhu M., Zhu G., Wu Z., Liu M., 2020. Spatial Variations of Subsurface Chlorophyll Maxima During Thermal Stratification in a Large, Deep Subtropical Reservoir. Journal of Geophysical Research: Biogeosciences. 125 (2): 1-13.
Liu Y., Xie F., Yang Z., Wei J.-E., Liao C., Chen W., Lü C., 2026. Iron-mediated photochemical fate of algal-derived DOM: Unraveling upward and downward environmental effects. Water Research. 291: 125234.
Liu Z., Dreybrodt W., Liu H., 2011. Atmospheric CO_2 sink: Silicate weathering or carbonate weathering? Quaternary Sciences. 31 (3): 426-430 (in Chinese).
Liu Z., Macpherson G. L., Groves C., Martin J. B., Yuan D., Zeng S., 2018. Large and active CO_2 uptake by coupled carbonate weathering. Earth-Science Reviews. 182: 42-49.
Lozupone C., Knight R., 2007. Global pattern in bacterial diversity. Proceedings of the National Academy of Sciences of the United States of America. 104: 11436-11440.
Lu X., Yu W., Chen B., Ma Z., Chen G., Ge F., An S., Han W., 2023. Imbalanced phytoplankton C, N, P and its relationship with seawater nutrients in Xiamen Bay, China. Marine Pollution Bulletin. 187: 114566.
Ma L., Huang X., Wang H., Yun Y., Cheng X., Liu D., Lu X., Qiu X., 2021. Microbial Interactions Drive Distinct Taxonomic and Potential Metabolic Responses to Habitats in Karst Cave Ecosystem. Microbiol Spectr. 9 (2): e0115221.
Meon B., Kirchman D. L., 2001. Dynamics and molecular composition of dissolved organic material during experimental phytoplankton blooms. Marine Chemistry. 75: 185–199.
Moody C. S., Worrall F., 2017. Modeling rates of DOC degradation using DOM composition and hydroclimatic variables. Journal of Geophysical Research: Biogeosciences. 122 (5): 1175-1191.
Murphy T. P., Hall K. J. Y., I., 1983. Coprecipitation of phosphate with calcite in a naturally eutrophic lake. Limnol. Oceanogr. 28: 58–69.
Newton R. J., Jones S. E., Eiler A., McMahon K. D., Bertilsson S., 2011. A Guide to the Natural History of Freshwater Lake Bacteria. Microbiology and Molecular Biology Reviews. 75 (1): 14-49.
Obernosterer I., Benner R., 2004. Competition between biological and photochemical processes in the mineralization of dissolved organic carbon. Limnology and Oceanography. 49 (1): 117-124.
Pu J., Li J., Zhang T., Martin J. B., Yuan D., 2020. Varying thermal structure controls the dynamics of CO2 emissions from a subtropical reservoir, south China. Water Research. 178: 115831.
Schuhmacher T., Loffler M., Hurler T., Takors R., 2014. Phosphate limited fed-batch processes:

https://doi.org/10.5194/egusphere-2026-4596
Preprint. Discussion started: 24 August 2026

impact on carbon usage and energy metabolism in Escherichia coli. J Biotechnol. 190: 96-104.
Shao M., Liu Z., Zeng S., Sun H., He H., Adnan M., Yan J., Shi L., Han Y., Lai C., Fang Y., 2025. Carbon sinks associated with biological carbon pump in karst surface waters: Progress, challenges, and prospects. Environmental Research. 267: 120712.
Shi X., Li W., Wang B., Liu N., Liang X., Yang M., Liu C.-Q., 2025. Keystone taxa drive the synchronous production of methane and refractory dissolved organic matter in inland waters. Water Research. 269: 122821.
Sterner R. W., Elser J. J., 2002. Ecological Stoichiometry. The Biology of Elements from Molecules to the Biosphere. Princeton University Press.
Sun L., Li J., Qu L., Wang X., Sang C., Wang J., Sun M., Wanek W., Moorhead D. L., Bai E., Wang C., 2023. Phosphorus limitation reduces microbial nitrogen use efficiency by increasing extracellular enzyme investments. Geoderma. 432
Syers J. K., Harris R. F., Armstrong D. E., 1973. Phosphate Chemistry in Lake Sediments. Journal of Environmental Quality. 2 (1): 1-14.
Tranvik L. J., Downing J. A., Cotner J. B., Loiselle S. A., Striegl R. G., Ballatore T. J., et al., 2009. Lakes and reservoirs as regulators of carbon cycling and climate. Limnol. Oceanogr. 54: 2298-2314.
Tu W., Xu J., Thompson I. P., Huang W. E., 2023. Engineering artificial photosynthesis based on rhodopsin for CO2 fixation. Nature Communications. 14 (1): 1-12.
Volk T., Hoffert M. I., 1985. Ocean Carbon Pumps: Analysis of Relative Strengths and Efficiencies in Ocean-Driven Atmospheric CO_2 Changes. The Carbon Cycle and Atmospheric CO_2: Natural Variations Archean to Present. 32: 99-110.
Wen Z., Shang Y., Song K., Liu G., Hou J., Lyu L., Tao H., Li S., He C., Shi Q., He D., 2022. Composition of dissolved organic matter (DOM) in lakes responds to the trophic state and phytoplankton community succession. Water Research. 224: 119073.
Woo P. C. Y., Lau S. K. P., Teng J. L. L., Tse H., Yuen K. Y., 2008. Then and now: use of 16S rDNA gene sequencing for bacterial identification and discovery of novel bacteria in clinical microbiology laboratories. Clinical Microbiology and Infection. 14 (10): 908-934.
Xamxidin M., Huang X., Yang X., Wang T., Chen C., Wu M., 2022. Limnobacter parvus sp. nov., a Thiosulfate-Oxidizing Bacterium Isolated from Lake Water. Current Microbiology. 80 (1): 1-7.
Yan W., Ji L., Yao Z., Yu Z., Kaikai Z., Xiaofei W., 2022. Denitrification Enhancement Effect and Microbial Floraanalysis of a new Biomass Carbon Source. Environmental Engineering. 40 (9): 63-117 (in Chinese).
Yang M., Liu Z., Sun H., Yang R., Chen B., 2016. Organic carbon source tracing and DIC fertilization effect in the Pearl River: Insights from lipid biomarker and geochemical analysis. Applied Geochemistry. 73: 132-141.
Yuan M. M., Guo X., Wu L., Zhang Y., Xiao N., Ning D., Shi Z., Zhou X., Wu L., Yang Y., Tiedje J. M., Zhou J., 2021. Climate warming enhances microbial network complexity and stability. Nature Climate Change. 11 (4): 343-348.
Yue G., Tinglin H., Nan L., Yunzhi Q., Fan S., Bin Y., 2022. Effect of Induced Mixing on Bacterial Community Structure and Metabolic Activity in Reservoir. Environmental Science. 43 (5): 2624-

https://doi.org/10.5194/egusphere-2026-4596
Preprint. Discussion started: 24 August 2026

2632.
Zevin A. S., Nam T., Rittmann B., Krajmalnik-Brown R., 2015. Effects of phosphate limitation on soluble microbial products and microbial community structure in semi-continuous Synechocystis-based photobioreactors. Biotechnology and Bioengineering. 112 (9): 1761-1769.
Zhang L., Zhong M., Li X., Lu W., Li J., 2020. River bacterial community structure and co-occurrence patterns under the influence of different domestic sewage types. Journal of Environmental Management. 266: 110590.
Zhang Z., Meng J., Chen Z., Zhou S., Zhang T., Chen Z., Liu Y., Cui J., 2023. Response of dissolved organic matter to thermal stratification and environmental indication: The case of Gangnan Reservoir. Science of The Total Environment. 868: 161615.
Zhou S., Sun Y., Zhang Y., Huang T., Zhou Z., Li Y., Li Z., 2020. Pollutant removal performance and microbial enhancement mechanism by water-lifting and aeration technology in a drinking water reservoir ecosystem. Science of The Total Environment. 709: 135848.